



OPEN ACCESS

EDITED BY

Anneliese Schrott-Fischer,
Innsbruck Medical University, Austria

REVIEWED BY

Jun-ming Tang,
Hubei University of Medicine, China
Takaomi Kurioka,
National Defense Medical
College, Japan
Bernd Fritsch,
The University of Iowa, United States
Lei Chen,
Vanderbilt University, United States

*CORRESPONDENCE

Gary D. Housley
g.housley@unsw.edu.au

SPECIALTY SECTION

This article was submitted to
Neuro-Otology,
a section of the journal
Frontiers in Neurology

RECEIVED 06 June 2022

ACCEPTED 24 August 2022

PUBLISHED 26 September 2022

CITATION

Cederholm JME, Parley KE, Perera CJ,
von Jonquieres G, Pinyon JL,
Julien J-P, Ryugo DK, Ryan AF and
Housley GD (2022) Noise-induced
hearing loss vulnerability in type III
intermediate filament peripherin gene
knockout mice.
Front. Neurol. 13:962227.
doi: 10.3389/fneur.2022.962227

COPYRIGHT

© 2022 Cederholm, Parley, Perera,
von Jonquieres, Pinyon, Julien, Ryugo,
Ryan and Housley. This is an
open-access article distributed under
the terms of the [Creative Commons
Attribution License \(CC BY\)](https://creativecommons.org/licenses/by/4.0/). The use,
distribution or reproduction in other
forums is permitted, provided the
original author(s) and the copyright
owner(s) are credited and that the
original publication in this journal is
cited, in accordance with accepted
academic practice. No use, distribution
or reproduction is permitted which
does not comply with these terms.

Noise-induced hearing loss vulnerability in type III intermediate filament peripherin gene knockout mice

Jennie M. E. Cederholm ¹, Kristina E. Parley ¹,
Chamini J. Perera ¹, Georg von Jonquieres ¹,
Jeremy L. Pinyon ¹, Jean-Pierre Julien ²,
David K. Ryugo ^{3,4,5}, Allen F. Ryan ^{6,7} and
Gary D. Housley ^{1*}

¹Translational Neuroscience Facility and Department of Physiology, School of Biomedical Sciences, UNSW Sydney, Sydney, NSW, Australia, ²Department of Psychiatry and Neuroscience, CERVO Brain Research Centre, Laval University, Quebec, QC, Canada, ³Garvan Institute of Medical Research, Sydney, NSW, Australia, ⁴School of Biomedical Sciences, UNSW Sydney, Sydney, NSW, Australia, ⁵Department of Otolaryngology, Head, Neck & Skull Base Surgery, St Vincent's Hospital, Sydney, NSW, Australia, ⁶Departments of Surgery and Neurosciences, University of California, San Diego, La Jolla, CA, United States, ⁷Veterans Administration Medical Center, La Jolla, CA, United States

In the post-natal mouse cochlea, type II spiral ganglion neurons (SGNs) innervating the electromotile outer hair cells (OHCs) of the 'cochlear amplifier' selectively express the type III intermediate filament peripherin gene (*Prph*). Immunolabeling showed that *Prph* knockout (KO) mice exhibited disruption of this (outer spiral bundle) afferent innervation, while the radial fiber (type I SGN) innervation of the inner hair cells (~95% of the SGN population) was retained. Functionality of the medial olivocochlear (MOC) efferent innervation of the OHCs was confirmed in the *Prph*KO, based on suppression of distortion product otoacoustic emissions (DPOAEs) via direct electrical stimulation. However, "contralateral suppression" of the MOC reflex neural circuit, evident as a rapid reduction in cubic DPOAE when noise is presented to the opposite ear in wildtype mice, was substantially disrupted in the *Prph*KO. Auditory brainstem response (ABR) measurements demonstrated that hearing sensitivity (thresholds and growth-functions) were indistinguishable between wildtype and *Prph*KO mice. Despite this comparability in sound transduction and strength of the afferent signal to the central auditory pathways, high-intensity, broadband noise exposure (108 dB SPL, 1 h) produced permanent high frequency hearing loss (24–32 kHz) in *Prph*KO mice but not the wildtype mice, consistent with the attenuated contralateral suppression of the *Prph*KO. These data support the postulate that auditory neurons expressing *Prph* contribute to the sensory arm of the otoprotective MOC feedback circuit.

KEYWORDS

cochlea, contralateral suppression, type II spiral ganglion neurons, medial olivocochlear (MOC) efferents, distortion product otoacoustic emission (DPOAE)

Introduction

Mammalian sound perception requires mechano-electrical transduction by cochlear inner hair cells (IHCs), each discretely innervated by multiple type I spiral ganglion afferent neurons (type I SGN). These afferents represent ~95% of the cochlear primary afferents synapsing in the cochlear nucleus region of the brainstem, where their synchronous firing in response to sound stimuli is evident as waves I and II of the evoked potential auditory brainstem response (ABR). The adjacent outer hair cells (OHCs) lend critical hearing sensitivity (~40 dB, or 100-fold) (1), converting sound-evoked receptor potentials into electromechanical force, amplifying and shaping basilar membrane vibration as a “cochlear amplifier” (2). OHC-specific electromotility can be directly measured as otoacoustic emissions using a sensitive microphone placed in the ear canal. The cochlear amplifier is subject to dynamic efferent neural feedback, which contributes broadly to hearing performance, including attention to sound, sound localization, hearing perception plasticity, improved hearing discrimination in noise, and protection of hair cells and their auditory synapses from acoustic overstimulation (otoprotection) (3, 4). The principal neural feedback circuit to the OHCs involves the contralateral medial olivocochlear (MOC) efferent neurons located within the superior olivary complex - ventral nucleus of the trapezoid body in the brainstem. MOC axons form the crossed olivocochlear bundle (COCB), which passes across the floor of the fourth ventricle, projecting to the ipsilateral cochlea, to synapse with the OHCs (5, 6). Through this MOC projection, contralateral acoustic stimulation strongly inhibits the ipsilateral cochlear amplifier (‘contralateral suppression’) (4, 7–9). It is generally thought that the sensory input from the contralateral cochlea driving the MOC feedback circuit arises from the IHC - type I SGN afferents (10, 11). This position is primarily founded on studies in guinea pig and cat where single MOC efferent fibers show recruitment from low sound levels (20 dB SPL), with sharp tuning curves and characteristic frequencies similar to those of adjacent type I SGN afferents (12, 13). However, evidence is emerging that at high sound levels, where MOC efferent feedback confers protection from noise-induced hearing loss (14), input from the OHC-type II SGN pathway may complement the IHC - type I SGN drive of the MOC efferent feedback circuit. For example, contralateral suppression was maintained following ouabain treatment of the cochlea that selectively ablated type I SGN (reducing ABR amplitude), while leaving the type II SGN innervation of OHCs intact (15). Further, type II SGN drive to the cochlear nucleus region known to connect with the MOC efferent arm of the circuit noise has recently been established for noise levels relevant to MOC efferent - mediated otoprotection (16).

The type II SGN are a small, enigmatic subpopulation (~ 5%) of unmyelinated afferents that exclusively innervate the OHCs (17, 18). Their peripheral neurites project radially past

the IHCs to form outer spiral bundles (OSB) that run basally, each branching to provide *en passant*, afferent synapses on multiple OHCs. This distributed receptive field overlaps with the frequency map of the cochlear amplifier, which spreads for ~¼ octave toward the basal (high frequency) region, corresponding to the active region of the cochlear amplifier (6, 19, 20). This is also congruent to a basal shift in the MOC efferent activation, which overlaps with the cochlear amplifier region as well as the type II SGN afferent map as sound levels increase (6, 21). The correspondence between the distribution of type II SGN afferent terminals and OHC-dependent active biomechanics prompted Kim (22) to propose that type II SGN contribute to the afferent input for the MOC efferent innervation of the OHCs.

In a prior study we investigated the afferent arm of the MOC feedback neural circuit using a peripherin knockout (*Prph*KO) mouse model (23). Peripherin is a type III intermediate filament protein associated with sensory fiber development, and in the mouse cochlea, peripherin expression is limited to the type II SGN post-natally (24, 25). The Froud et al. (23) study demonstrated disruption of the type II SGN innervation of the OHCs and an associated attenuation of contralateral suppression. A subsequent examination of the *Prph*KO mouse model challenged the morphological phenotype and postulated that the reported disruption of the MOC reflex may have been due to selective effects of loss of *Prph* expression by MOC neurons (11). In the present study we show that the IHC - type I SGN afferents and MOC efferent fibers remain viable in the *Prph*KO mouse model, while the disruption of the type II SGN afferent innervation of the OHC in *Prph*KO mice is more profound than indicated in our initial report (23). This selective disruption of the afferents innervating the cochlear amplifier is associated reduction in the MOC efferent reflex and loss of otoprotection from acoustic overstimulation.

Materials and methods

Animals

Male and female adult 129Sv/C57BL/6 wildtype (WT) and *Prph*-null (*Prph*KO) mice on the same background were used for this study. For acoustically-evoked contralateral suppression hearing studies, and noise-induced hearing loss studies, mice were anesthetized using intraperitoneal injections (i.p.) of a ketamine (40 mg/kg)/xylazine (8 mg/kg)/acepromazine (0.5 mg/kg) (k/x/a) cocktail. Further k/x/a was administered (half the initial k/x/a dose mixed with the equivalent volume of 0.9% saline) as required to keep the mice anesthetized throughout the experiment (typically every 30 min). For the electrically-evoked MOC stimulation experiments mice were anesthetized with an initial k/x/a injection as above, then kept anesthetized with 0.5–1% isoflurane supplemented with O₂ throughout the experiment. The level of anesthesia and the O₂ saturation of the

mice were monitored using a pulse oximetry system (MouseOx, STARR Life Sciences, SDR Scientific, Australia). Mice were kept on a heat pad for the duration of the experiment with their core body temperature clamped at 37°C by feedback control (Right Temp, Able Scientific, Perth, Australia). Ophthalmic ointment was applied to the eyes once the animal was anesthetized to prevent corneal drying. At the completion of the studies, the animals were euthanised using pentobarbital (Virbac Australia, 100 mg/kg of body weight at 100 mg/ml, i.p.). Experiments were conducted according to UNSW Sydney Animal Care and Ethics Committee approved protocols, which conform to the Australian code for the care and use of animals for scientific purposes (26). The design and communication of the study align with the ARRIVE guidelines (27).

Genotyping

The *Prph*KO mouse model was established in 2001 using 129Sv strain embryonic stem cells bearing the peripherin knockout construct (exon 1 deletion) that were injected into C57BL/6 strain blastocysts (28). To produce heterozygous *Prph*KO mice, the generated chimeric mice were crossed with C57BL/6 mice. These heterozygous mice were used as breeders to provide littermates of identical genetic background. The *Prph*KO mouse line was established at UNSW in 2008. PCR-based genotyping utilized the following primer sets: *Prph*-5'-UTR-F: 5' GCT ATA AAG CCG CCC CGC ATC 3'; *Prph*-exon1-R: 5' AGG GCT GCG TTC TGC TGC TC 3'; *LacZ*-R: 5' GTC CTG GCC GTA ACC GAC CC 3'; Imaging of the PCR amplicons following agarose gel electrophoresis was used to distinguish WT (452 bp), KO (640 bp) and heterozygous (452 + 640 bp bands) mice (Supplementary material 1A). Homozygous knockout genotype validation was confirmed by the absence of peripherin immunolabelled cochlear type II SGN [after (23)] (Supplementary material 1B,C).

Immunohistochemistry

Mouse cochleae were dissected and fixed by scali perfusion of 4% paraformaldehyde, decalcified for 14 days in 8% EDTA and then cryoprotected using 30% sucrose. The cochleae were mounted (Optimum Cutting Temperature (O.C.T) compound, Tissue-Tek, Sakura Finetek, Torrance, CA, USA) and cryosectioned at 50 µm. For wholemount preparations, cochleae were dissected into 2–4 pieces at the apical and basal turns. In both free-floating cryosections and the wholemounts, non-specific binding was blocked with 10–15% normal goat or donkey serum, 1 % Triton X–100 in phosphate buffered saline (PBS) for 1 h at room temperature (RT). Sections were then immersed in primary antibodies: Neurofilament heavy polypeptide (NF200, Sigma, Cat# N4142, RRID: AB_477272; rabbit, 1:5000); C-terminal-binding protein

2/RIBEYE ribbon synapse maker (29) (CtBP2, BD Bioscience, Cat# 612044, RRID: AB_399431; mouse, 1:500); Tubulin beta-3 chain (β-III tubulin) (TuJ1, Covance, Cat# MMS-435P, RRID: AB_2313773; mouse, 1:1000); Peripherin (Everest Biotech, Cat# EB12405, RRID: AB_2783842; goat, 1:1000); Parvalbumin alpha (Swant, Cat# PVG-213, RRID: AB_2650496; goat, 1:1000); Vesicular acetylcholine transporter (VACht) (Phoenix Pharmaceuticals Inc., Cat# H-V007, RRID: AB_2315530; rabbit, 1:100); Myosin 7A (Proteus, Cat# 25-6790, RRID: AB_10015251; rabbit, 1:500); AMPA subtype 2 glutamate receptor (GluA2, Millipore, Cat# MAB397, RRID: AB_2113875; mouse, 1:1000) in 5–10% normal goat or donkey serum, 0.1% Triton X - 100 in PBS, overnight at RT. Sections were then washed in PBS and appropriate secondary antibody was applied overnight at RT [anti-rabbit IgG AlexaFluor 594, anti-mouse IgG AlexaFluor 488/594/647 (1:1000) or anti-goat IgG AlexaFluor 488 (1:1000) (Molecular Probes)], 5% normal goat or donkey serum in PBS. Following a further PBS wash, nuclear labeling was achieved by incubating the sections for 5 min in DAPI (4',6-diamidino-2-phenylindole; 1:5000; Sigma). Two final washes in PBS were performed before the sections were mounted on glass slides using Vectashield (Vector Laboratories) and imaged on a Zeiss confocal microscope (Zeiss 710 NLO). Data were obtained from 1–3 organ of Corti z stacks (30 µm) analyzed per animal, typically 3 animals per group. Data for the quantitative analysis of ribbon synapses was obtained using 30 µm stacks of confocal images; 63x oil immersion objective; mid-cochlear level, parsing the position of the CtBP2-labelled puncta within 2.5 µm bins relative to the equator line of the DAPI-labelled OHC nuclei. These data were blinded, randomized, and double scored before decoding.

Hearing function tests

Hearing testing was carried out in a sound-attenuating chamber (Sonora Technology, Japan) using an auditory-evoked potential and DPOAE workstation (TDT system 3 with RX6 and RX6-2 signal processors, Tucker Davis Technologies, Ft Lauderdale, FL, USA) with BioSig32 software. Sound levels were calibrated using a one-quarter-inch Free Field Measure Calibration Microphone (model 7016; ACO Co Ltd., Japan).

Acoustically-evoked contralateral suppression

The contralateral ear was exposed to broadband suppressor sound stimulation (96 dB SPL noise, 15–25 kHz, 15 s; $n = 7$ each for WT and *Prph*KO; 82 dB SPL noise, 10–17 kHz, 60 s; $n = 8$ each for WT and *Prph*KO) using a MF1 speaker (TDT), while cubic ($2f_1-f_2$) DPOAEs were detected using a microphone coupled to the ipsilateral ear canal (ER-B10+, Etymotic Research, IL, USA), alongside two EC1 electrostatic speakers (TDT), controlled by the TDT system 3 workstation. DPOAEs were elicited using equal primary tones (f_1 and f_2 ;

f_2/f_1 ratio: 1.25) around 20 kHz at 60 dB (for the 96 dB SPL noise study) or around 28 kHz at 65 dB (for the 82 dB SPL noise study). In total 10–50 measurements were averaged (6.7/s) for each recording. DPOAE measurements were taken before (baseline), during and following (recovery) suppressor stimulus.

Electrically-evoked contralateral suppression

To directly drive the contralateral MOC efferent innervation of the OHCs, these fibers were electrically stimulated at the point where they cross the midline on the floor of the fourth ventricle of the brainstem. Mice were initially anesthetized with a k/x/a cocktail, maintained on a heat pad and eye ointment applied as described in the section *Animals*. This was followed by shaving the head to provide a clean surgical field for the dorsal-occipital approach to the fourth ventricle. A tracheostomy was performed, and the animals were ventilated throughout the experiment with a respiration rate of 100 breaths per minute and 10 cm peak inspiratory pressure (Kent Scientific TOPO™ Dual Mode Ventilator, Torrington, CT, USA). The animal was then positioned onto a teeth bar to stabilize the head position. The dorsal brainstem was accessed by removing muscles and connective tissue between the C1 (Atlas) vertebra and the occiput. This was followed by an incision in the dura covering the foramen, and the stimulating electrodes (two platinum iridium wires with 500 μm exposed tips, 400 μm separation) were positioned with one electrode on the midline of the fourth ventricle floor and the second electrode ipsilateral, using a micromanipulator. Twitching of the ears in response to a test electrical stimulation (monophasic 150 μs pulses, 200 Hz) \sim 5s, indicated the correct position. α -D-tubocurarine (1.25 mg/kg, i.p.) was then administered to achieve muscle paralysis, which included paralysis of the stapedius reflex. The right (ipsilateral) external auditory meatus of the mouse was coupled to the DPOAE probe. A baseline measurement was obtained as the cubic DPOAE around 16 kHz at 50 or 55 dB SPL primaries ($f_1 = f_2$ amplitude, producing DPOAEs \sim 10 dB above the noise floor); 20 averaged measurements (10 samples each) over 1 min. The electrically-evoked contralateral suppression was then recorded during 25 seconds of stimulation (8 data point averages), followed by 2.5 min of recorded recovery. The DPOAE amplitudes were analyzed relative to the noise floor. These experiments proved particularly challenging, with 3/16 WT mice and 3/7 *Prph*KO mice providing useable data. However, electrically-evoked DPOAE suppression for each of the successful WT and *Prph*KO mice ($n = 3$ mice per genotype) were obtained from 3–5 repeats per mouse.

Comparison of vulnerability to noise-induced hearing loss

To assess the otoprotection conferred by OHC–type II SGN–mediated MOC efferent cochlear amplifier suppression,

noise-induced hearing loss was assessed in *Prph*KO vs. WT mice using auditory brainstem responses (ABRs) and cubic DPOAE measurements with acute noise presentation. For ABR, following k/x/a anesthesia induction, subdermal platinum electrodes were inserted subcutaneously at the vertex (+), over the mastoid process (–), and in the hind flank (ground) [after (30)]. Click (100 μs alternating polarity) or pure tone pips (4, 8, 16, 24, and 32 kHz) stimuli (5 ms, 0.5 ms rise/fall time, 10/s) were delivered using an EC1 electrostatic speaker, with the generated ABR potentials amplified, filtered and averaged 512 times using the TDT System 3 workstation. The ABR threshold for each frequency was determined as the lowest intensity (5 dB steps from 70 dB SPL) at which the P2 ABR wave could still be visually observed above the noise floor (\sim 100 nV). Cochleae were then exposed to 108 dB SPL “open field” broadband white noise (4–32 kHz; 2nd order Bessel filter) for 1 h. The white noise stimulus was generated using custom software with a National Instruments A/D driving an amplifier (BIEMA model Q250, Altronic, Northbridge, WA, Australia) and delivered *via* an MF1 speaker (TDT) positioned at midline, 15 cm in front of the mouse ($n = 9$ for each genotype). The noise was calibrated at ear level. ABR threshold shifts were determined immediately post-noise by remeasurement before the mice recovered from the anesthesia. The mice were then rested for 14 days before being re-tested to determine sustained hearing loss [permanent threshold shift (PTS), after (31)].

Data analysis

Data are presented as the population mean \pm s.e.m.. Statistical analysis was performed using a one-way Analysis of Variance (ANOVA), a two-way repeated measures (RM) ANOVA (Sigmaplot®, Systat Software Inc., San Jose, CA, USA), a two-way ANOVA or *t*-test, as indicated; significance at $\alpha \leq 0.05$. Data were tested for normal distribution and Holm-Sidak *post hoc* analysis was utilized for multiple pairwise comparisons within ANOVA. Grubbs’ test was used to assess data outliers (GraphPad software, San Diego, CA, USA). Data were graphically presented using Sigmaplot® software.

Results

Disruption of the outer spiral bundle (type II SGN) fiber tracts in *Prph* knockout cochleae

The type II SGN somata sub-population was specifically identified using peripherin immunofluorescence. The neurons were predominantly located in the lateral aspect of Rosenthal’s canal, juxtaposed to the intraganglionic spiral bundle of efferent fibers ($n = 6$ WT). As previously reported (23),

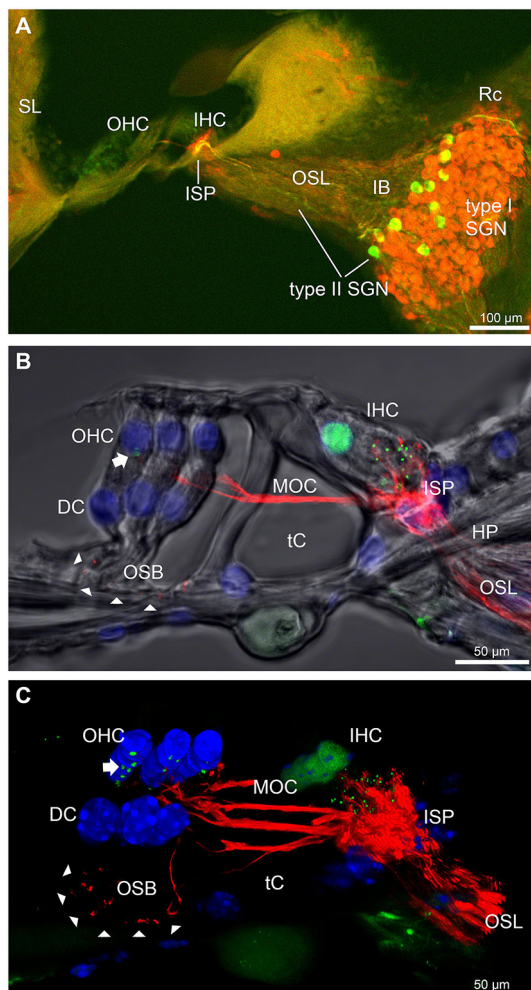
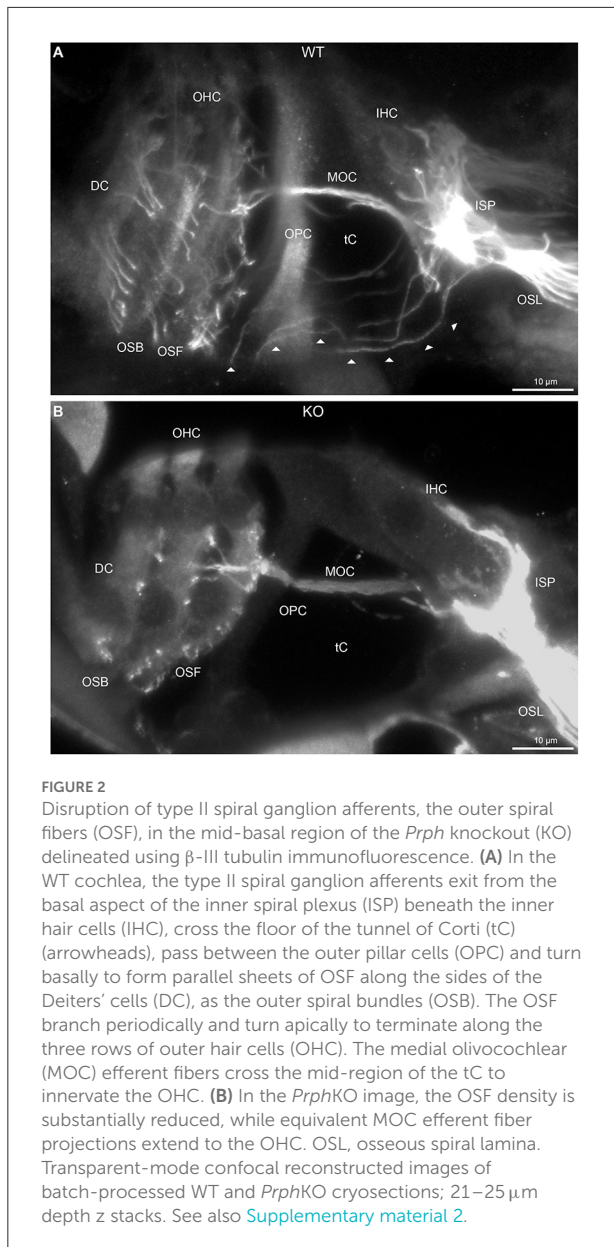


FIGURE 1
Immunofluorescence labeling of the afferent and efferent innervation of the organ of Corti in the wildtype mouse cochlea. **(A)** Spiral ganglion neuron (SGN) somata and neurites (type I SGN (red) β -III tubulin immunofluorescence; type II SGN (green/yellow) peripherin immunofluorescence). The type II SGN sub-population is biased to the lateral aspect of Rosenthal's canal (Rc), proximate to the intraganglionic spiral bundle (IB); the IB contains the medial olivocochlear (MOC) efferent axons from the superior olivary complex of the brainstem. All three nerve fiber types project to the organ of Corti via the osseous spiral lamina (OSL). The inner spiral plexus (ISP) is located at the basal pole region of the inner hair cells (IHC) and predominantly reflects type I SGN terminals. OHC, outer hair cells; SL, spiral ligament. **(B)** Detail of the innervation and pre-synaptic ribbon complexes of the hair cells within the organ of Corti, delineated using NF200 (red) immunofluorescence for the nerve fibers and CtBP2/RIBEYE (green) immunofluorescence for the ribbons. Single confocal optical section overlaid with transmitted light image. NF200 immunolabelling delineates type II SGN neurites as discrete outer spiral bundle (OSB) fiber tracts (delineated by arrowheads) beneath the OHCs and their supporting Deiters' cells (DC). Nuclei labelled with DAPI (blue). MOC efferent fibers cross the tunnel of the organ of Corti (tC) to innervate the OHCs. Note synaptic ribbons basal to the OHC nuclei (arrow). In comparison, the sub-nuclear domain of the IHCs contains many more CtBP2 immunopositive synaptic ribbons, each of which is
(Continued)

FIGURE 1 (Continued)
aligned to a single type I SGN neurite terminal. Habenula perforata (HP). **(C)**, Confocal immunofluorescence reconstruction of a 50 μ m cryosection delineates cell structure within the organ of Corti. The CtBP2 immunopositive synaptic ribbons are localized in a highly regular pattern beneath the mid-ventral aspect of the OHC nuclei (one or two per OHC; arrow), whereas each IHC contains > 10 CtBP2 puncta. The type II SGN outer spiral fibers within the OSB are clearly delineated (arrowheads) by the NF200 immunofluorescence ventral to the DCs. See also [Supplementary material 2](#) for 3D rendering.

the anti-peripherin fluorescence signal declined with age, particularly in the peripheral neurites (see adult WT cochlea [Figure 1A](#); and post-natal day 8 cochlea ($n = 3$ WT), [Supplementary material 1C](#)). β -III tubulin and NF200 immunolabelling was employed for comparison of the representation of type I and type II SGN neurite projections within the adult mouse cochlea across wildtype (WT) and *Prph*KO tissue ([Figures 1A–C](#); [Supplementary material 2](#)). The type II neurites track alongside the type I radial fibers within the osseous spiral lamina. Both types of afferent neurites pass through the habenula perforata and project toward the base of the inner hair cells (inner spiral plexus, ISP). The β -III tubulin and NF200 immunofluorescence labelled type II SGN neurites extended beyond the inner hair cells, with the fibers crossing the tunnel of Corti well beneath the extensive medial olivocochlear (efferent) bundle fibers (MOC) ([Figures 1–4](#); [Supplementary material 3](#)). The type II fibers then became basally projecting outer spiral fibers within the OSB beneath each of the three rows of OHCs and their associated Deiters' cells (DC). The outer spiral fibers periodically separate from the OSB, to ascend between the DC processes and make afferent synapses at the bases of OHCs (for example, [Figures 1B,C, 2A](#)).

In *Prph*KO cochleae, the immunolabelling of the type II SGN afferent innervation was distinctly disrupted, whereas the type I SGN innervation and the MOC efferent fiber representation were normal in appearance. Comparisons between *Prph*KO tissue and corresponding WT tissue utilized batch immunoprocessing and imaging ([Figures 2–4](#); [Supplementary material 3](#); [Supplementary material 4](#); [Supplementary material 5](#)). In *Prph*KO, both β -III tubulin ([Figure 2A](#) for WT compared with [Figure 2B](#) for *Prph*KO, mid-basal region; [Figures 3A,C](#) for WT and [Figures 3B,D](#) for *Prph*KO apical and mid-regions) and NF200 ([Figure 4A](#) WT apical compared with [Figure 4B](#) *Prph*KO apical, with [Figure 4C](#) WT basal compared with [Figure 4D](#) *Prph*KO basal) labeling delineated a residual population of outer spiral fibers projecting from the ISP region, across the floor of the tunnel of Corti, and out to the OSBs in both whole-mount ($n = 3$ WT, $n = 5$ KO) and cryosectioned tissue ($n = 6$ WT, $n = 4$ KO). There was an evident gradient in this OSB pathology along the length of the organ of Corti, from an almost complete loss of these



type II afferent fibers at the apex [see [Figure 4B](#) (*Prph*KO) compared with [Figure 4A](#) (WT) for apical region where OSB loss is extensive], to a partial retention of OSB fibers in the basal region [compare [Figure 4D](#) (*Prph*KO) vs. [Figure 4C](#) (WT); [Supplementary material 6](#)]. It could not be established whether this reduction in outer spiral fiber number reflected atrophy of the peripheral neurite processes of the type II SGN, or arose from loss of type II SGN cell bodies, because the peripherin immunolabelling was intrinsically absent in the *Prph*KO. However, the OSB remodeling clearly reflected disruption of the sensory neural drive from the OHCs.

While clearly resolving the type II SGN afferent fibers as OSB, neither of the neuron-specific antibodies (β -III tubulin, NF200) delineated the terminal region of these fibers at the

OHCs, likely reflecting limited trafficking of the β -III tubulin or the neurofilament 200 proteins to the synaptic region. Parvalbumin immunolabelling was therefore used to probe type II fiber terminations at the OHCs. Parvalbumin is a calcium binding protein that is expressed by type I and type II SGN, as well as the hair cells and supporting cells of the organ of Corti ([11](#)). This further resolved the disruption of the OHC afferent innervation, where the density of these outer spiral fiber terminal processes was substantially diminished in the *Prph*KO tissue [[Figure 5A](#) (WT apical region) compared with [Figure 5B](#) (*Prph*KO apical); [Figure 5C](#) (WT basal) compared with [Figure 5D](#) (*Prph*KO basal) ($n = 2$) *Prph*KO, batch processed with WT tissue ($n = 3$)].

Dysregulation of the outer hair cell pre-synaptic ribbon complexes in *Prph* knockout cochleae

CtBP2/RIBEYE and NF200 dual immunolabelling of *Prph*KO cochleae showed disruption of the ordered structure of the synaptic ribbon complexes at the base of the OHCs, juxtaposed to the type II SGN afferent neurite terminals. As evident in [Figures 1C, 4A,C, Supplementary material 2](#), 1–2 CtBP2 positive puncta are normally present in the mid-basal region of each of the WT OHC, beneath the nucleus; in the *Prph*KO tissue, this regular pattern was lost ($n = 2$ WT and 2 *Prph*KO cochleae, 15–19 weeks of age; batch-processed; [Figure 6A](#) is an optical section showing the typical WT OHC synaptic ribbon location on the basolateral aspect of the OHC; [Figure 6B](#) is an example of the apical drift of these synaptic ribbons in the *Prph*KO OHCs). This abnormality was elaborated by dual immunolabelling for CtBP2 and the vesicular acetylcholine transporter (VACHT), which marks the synaptic boutons of the MOC efferent innervation of the OHCs ([Supplementary material 7](#)). In both WT ($n = 5$) and *Prph*KO ($n = 3$) mice, multiple large VACHT positive efferent boutons are present at each OHC, on the medial and mid region of the basal pole of the cells, indicating retention of the efferent MOC innervation of the OHC. In 1–3 CtBP2-labelled pre-synaptic ribbons were interposed with the MOC synapses or occupied the lateral aspect of the synaptic pole of the WT OHCs. In the *Prph*KO cochleae, the apical displacement of many of the synaptic ribbons relative to the base of the OHC was comparable to the initial CtBP2 immunolabelling study. This dislocation of the ribbon synapses was selective for the *Prph*KO OHCs, as CtBP2 and VACHT labeling of the IHC/ISP regions were comparable between WT and *Prph*KO cochleae.

Displacement of CtBP2-immunolabelled hair cell ribbon synapses is a primary marker of deafferentation ([32](#)) and analysis of the location of the ribbons provided an objective

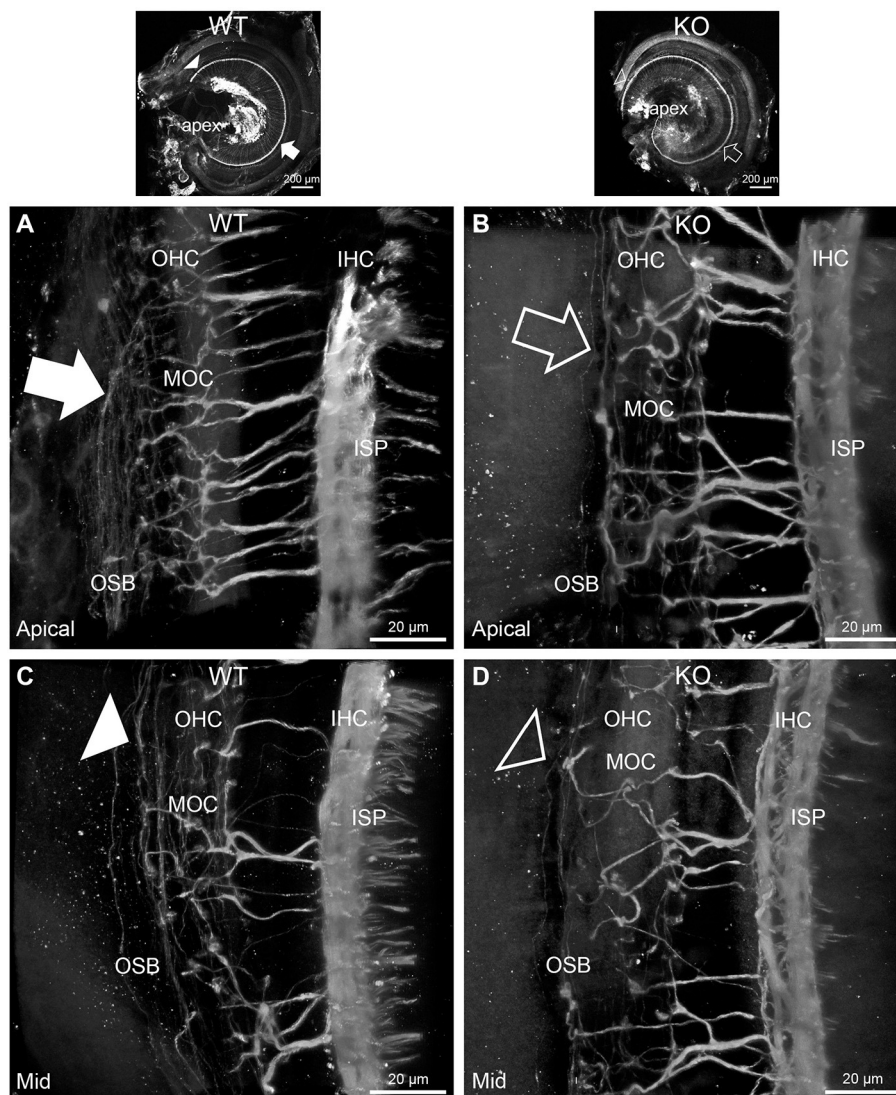


FIGURE 3

Disruption of the outer spiral bundle structure (OSB; type II spiral ganglion neurites form the outer spiral bundles) in *Prph* knockout (KO) vs. wildtype (WT) mouse cochleae from apex to mid region. Arrows in the low-power images indicate the corresponding regions of these whole-mount preparations which are shown at high resolution. The outer spiral fibers run parallel to the tunnel of Corti within the OSB (arrows), whereas the MOC fibers project across the tunnel from the inner spiral plexus (ISP) region to the outer hair cell (OHC) region, where they branch to innervate multiple OHCs. Note the comparatively higher number of outer spiral fibers in the apical region in the WT (**A**) (filled arrow), compared with the mid-cochlear region in the same tissue (**C**), (filled arrowhead). The corresponding regions in the wholemount KO cochlea (**B,D**); (open arrow and open arrowhead) show minimal labeling in the OSB. Note the equivalency between KO and WT, of the medial olivocochlear (MOC) efferent axon projections to the OHCs. Maximum intensity projection β -III tubulin immunofluorescence confocal images of the organ of Corti (imaged from the basilar membrane surface to optimally resolve the OSB). IHC, inner hair cell region. See also [Supplementary materials 4, 5](#) for 3D rendering.

assessment of the disruption of the *Prph*KO type II SGN afferent synapses with the OHC. The location of the OHC pre-synaptic ribbon complexes was quantified by batch-processing WT and *Prph*KO cryosections and undertaking a blinded measurement and analysis of the distance of the CtBP2 puncta relative to the equator line of OHC nuclei in z stacks of optical sections using a 63x oil-immersion objective, with measurement of 13–57

OHC ribbons in cryosections from each of 5 WT mice (total 175 ribbons) and 6–60 ribbons from cryosections from each of 6 *Prph*KO mice (total 214 ribbons) ([Figure 6C](#) shows the ribbon distribution relative to the nucleus equator) (see also [Supplementary material 8](#)). Overall, the average CtBP2 puncta location in WT was $1.81 \pm 0.24 \mu\text{m}$ below the OHC nucleus equator, compared with $0.53 \pm 0.36 \mu\text{m}$ above the OHC nucleus

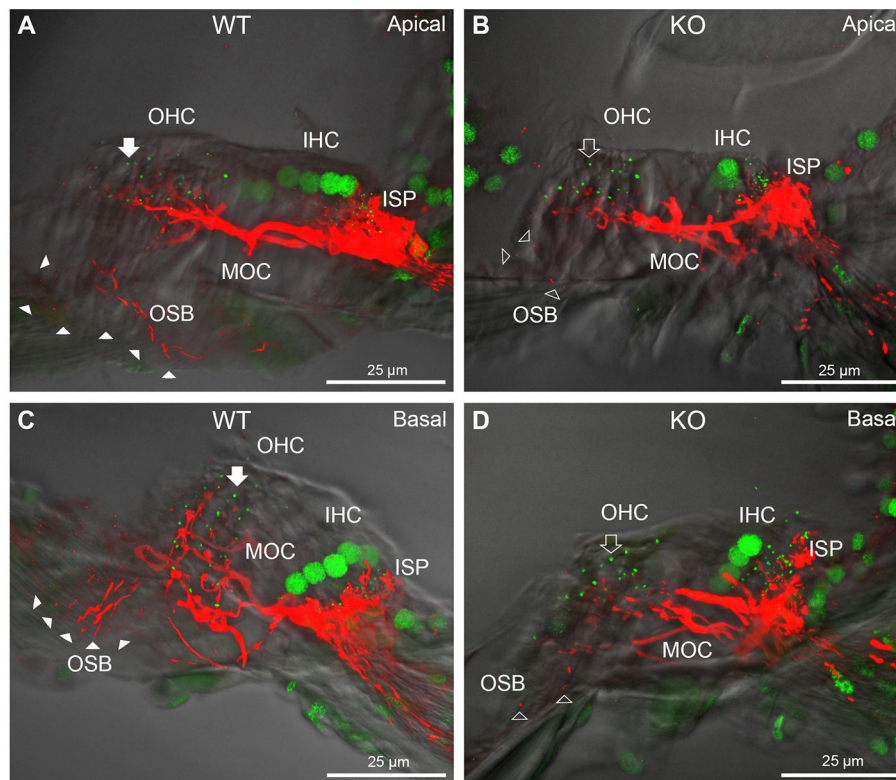


FIGURE 4

Comparison of NF200 (red) immunolabelling of outer spiral bundle (OSB) structure of the type II SGN neurites projecting to the outer hair cells (OHC) from wildtype (WT, filled arrow heads) and *Prph*KO (open arrow heads) cochleae. Note the limited OSB representation in the KO tissue from all regions. Images from single mid-modiolar cryosections for each of WT and KO illustrate the OSB fiber density within the organ of Corti at the apex (A,B) and base (C,D). CtBP2/RIBEYE immunofluorescence (green puncta) delineates the pre-synaptic ribbons in both the OHCs and inner hair cells (IHC). The regular pattern of pre-synaptic ribbons at the mid-basal region of the three rows of OHCs evident in the WT (filled arrow), is disrupted in the KO (open arrow). The medial olivocochlear (MOC) efferent fiber innervation of the OHCs lies above the OSB. The dense type I SGN fiber synaptic complex at the base of the IHC (inner spiral plexus, ISP) is juxtaposed to the high density of synaptic ribbons in both WT and KO tissue. In total 50 μm cryosections; confocal projection images. See also [Supplementary material 6](#).

equator for the *Prph*KO. This apical migration of the ribbons in *Prph*KO OHCs compared with the average location of the ribbon synapses in the WT OHCs was highly significant. In WT OHC, only $16.5 \pm 5.4\%$ of the CtBP2 immunopositive synaptic ribbons were located above the nucleus equator, whereas in the *Prph*KO mice this increased to $41.9 \pm 3.6\%$ (Figure 6D; $p = 0.00313$, t -test); indicative of disruption of synaptic integrity with the type II SGN afferent terminals in the *Prph*KO.

Acoustically-evoked contralateral suppression in the *Prph* knockout mouse

The phenotype of loss of contralateral suppression in the *Prph*KO mice reported by Froud et al. (23) was based on measurement of quadratic DPOAE (f_2 - f_1) amplitude changes.

This was validated in the current study using the cubic ($2f_1$ - f_2) DPOAE (Figures 7A–D), which is sensitive to changes in the gain of the cochlear amplifier (33, 34), as mediated by MOC efferent drive. There was no difference in the baseline sensitivity of OHC electromechanical transduction in WT and *Prph*KO mice [reflected as equivalent cubic DPOAE amplitudes with 60 dB SPL f_1/f_2 drivers; Figure 7A (WT upper trace compared with KO lower trace)]. In WT mice, presentation of broad band white noise at 96 dB SPL (15 s; Figure 7C) or 82 dB SPL (60 s; Figure 7D) to the left ear produced robust reductions in the cubic DPOAE recorded in the right ear (contralateral suppression), which largely adapted within 15 s. For 96 dB SPL contralateral noise, with 60 dB SPL pure tone drivers around 20 kHz in the ipsilateral ear, the peak noise-induced reduction in DPOAE in WT mice was -11.5 ± 3.0 dB ($n = 7$), measured 3 s after noise onset (Figure 7C). In contrast, only a residual contralateral suppression effect was detected in the *Prph*KO mice at this level (peak = $-1.6 \pm$

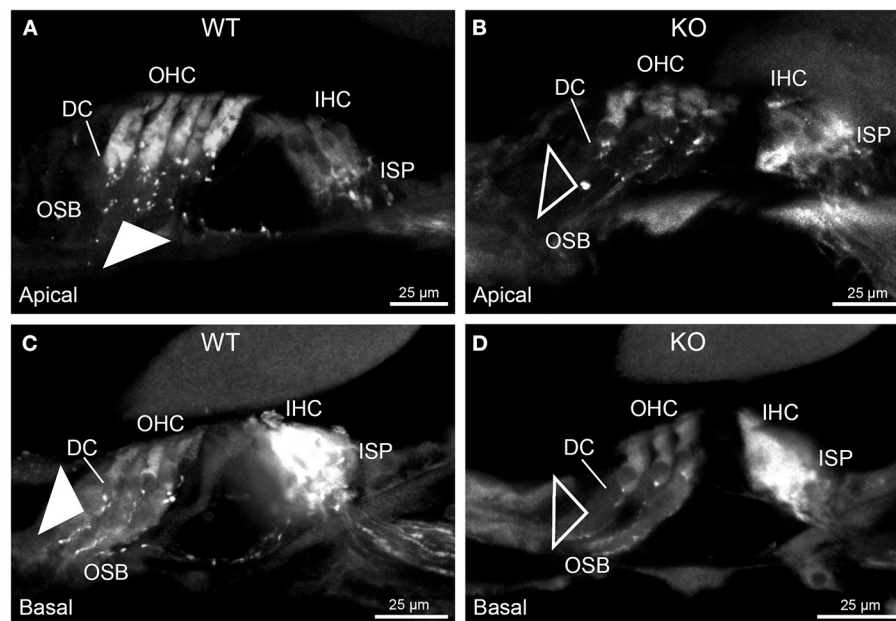


FIGURE 5

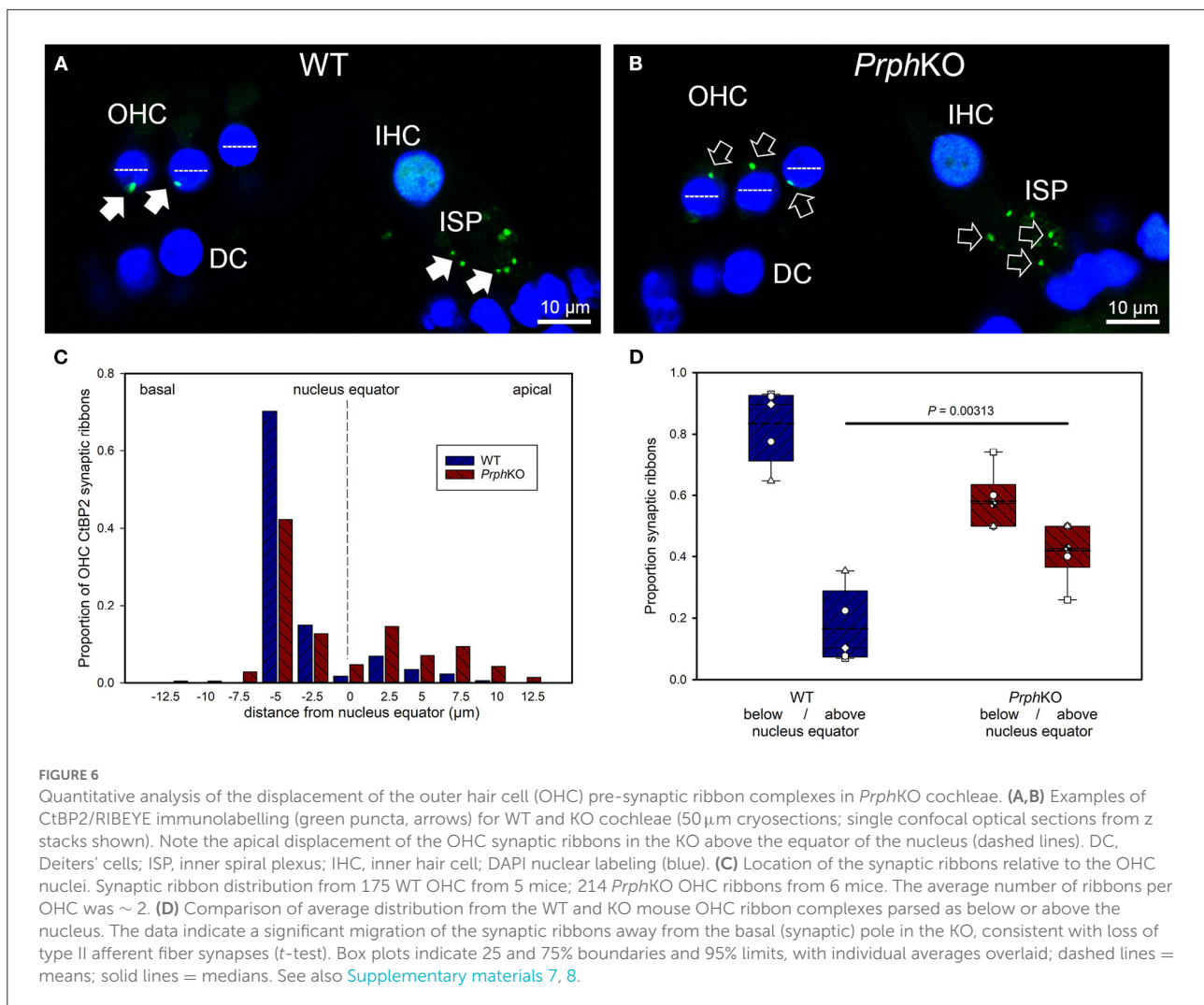
Parvalbumin immunofluorescence resolves the disruption of the type II SGN fibers (outer spiral fibers) within the outer spiral bundles (OSB) of the *Prph*KO mouse cochlea. Examples of batch-processed cryosections from WT (A,C) and KO (B,D) cochleae delineate the terminal regions of the outer spiral fibers, particularly with respect to their migration along the medial aspect of the Deiters' cells (DC) up to the base of the outer hair cells (OHC). Parvalbumin was also strongly labelled in the inner hair cells (IHC) in the basal region of the cochlea (C,D), and in type I SGN afferent fibers within the inner spiral plexus (ISP). There was a much higher density of outer spiral fiber labeling at the level of the OSB in the WT tissue (filled arrowheads) compared with the KO tissue (open arrowheads), consistent with the β -III tubulin and NF200 immunolabelling experiments. The medial olivocochlear efferent projections to the OHCs are not delineated by this parvalbumin immunolabelling. Apical and basal regions from the same cochlea for each of WT and KO.

1.6 dB; $p = 0.003$, one sample *t*-test, $n = 7$). The difference in peak contralateral suppression between WT and *Prph*KO mice with the 96 dB SPL noise presentation was therefore 9.9 dB ($p = 0.013$; unpaired *t*-test). The peak contralateral suppression in the WT mice with 82 dB SPL noise (65 dB SPL drivers around 28 kHz) was -3.5 ± 1.3 dB, measured at 6 s after noise onset (Figure 7D). There was no significant contralateral suppression in the *Prph*KO mouse group at any sample period with 82 dB SPL noise presentation (e.g., -0.2 ± 0.1 dB at 6 s, $p = 0.379$). The 3.3 dB difference in peak DPOAE suppression at this noise level between WT and *Prph*KO at 6 s was significant ($p = 0.026$, unpaired *t*-test; $n = 8$ per genotype).

Validation of the viability of the medial olivocochlear efferent drive to the outer hair cells in the *Prph* knockout mouse by electrical stimulation

Direct electrical stimulation of the COCB efferent fiber track at the floor of the fourth ventricle was performed to

eliminate the possibility that the loss of acoustically-evoked contralateral suppression in the *Prph*KO mice was due to disruption of the MOC efferent drive to the OHCs. Electrical stimulation of the MOC efferent fibers as they cross the floor of the fourth ventricle in the brainstem was used to directly compare the strength of the motor drive to the ipsilateral OHCs, assessed as cubic DPOAE suppression in WT vs. *Prph*KO mice. This physiological preparation required stable presentation of DPOAE following a craniotomy to access the fourth ventricle, and precise micro-positioning of the bipolar stimulating electrodes, with one electrode at the mid-line, ~ 0.2 mm rostral to the obex, and the second electrode positioned ~ 0.4 mm lateral, toward the ipsilateral cochlea. Transient test stimuli were used with repositioning of the probe, until suppression of the cubic DPOAE was observed. The stimulus voltage was then lowered below threshold (~ 3 V) and a series of recordings were obtained as the stimulus intensity was progressively stepped up to a maximum of 10 V, with 4-min recovery intervals between tests. The responses peaked within 12 s, with no substantial adaptation out to 25 s stimulation in both *Prph*KO and WT mice. Figure 8A shows an example of establishment of the stimulus threshold for electrically-evoked contralateral suppression in a *Prph*KO mouse. For statistical



comparison, the amplitudes of electrically-evoked DPOAE suppression measurements at suprathreshold voltages were used (3 repeats for WT, 3–5 repeats for *Prph*KO to determine the average response for each mouse) (Figure 8B). The average reduction in DPOAE amplitude during the 25 s stimulus from these trials was then used for statistical comparison between genotypes (Figure 8C). A repeated measures two-way ANOVA showed that the sensitivity of the electrically-evoked contralateral suppression was equivalent between *Prph*KO and WT mice (WT = -2.7 ± 0.3 dB, $n = 3$; KO = -2.6 ± 0.2 dB, $n = 3$; $p = 0.534$). The need for precise positioning of the stimulus probe to achieve an electrically-evoked change in DPOAE is demonstrated in Figure 8A, where a repositioning of the probe “off-target” eliminated the DPOAE suppression. There was no difference in the amplitudes of the baseline cubic DPOAE in the WT and *Prph*KO cochleae, WT average = 17.1 ± 0.3 dB above noise-floor; KO = 16.1 ± 0.2 dB; $p = 0.078$; unpaired *t*-test).

Loss of otoprotection from noise-induced hearing loss in *Prph* knockout mice

Reduction of OHC electro-mechanical transduction by the MOC efferent pathway is otoprotective (14, 35). For example, surgical ablation of the COCB at the floor of the fourth ventricle in cats increased noise-induced threshold shifts (36) and over-expression of the OHC $\alpha 9$ nicotinic acetylcholine receptor subunit in mice confers protection to noise-induced hearing loss (NIHL) (37). Here we investigated the effect of disruption of the OHC–type II SGN sensory input arising from knockout of *Prph* in this key aspect of hearing homeostasis. The vulnerability to 1 h of acute white noise (4–32 kHz) at 108 dB SPL was assessed in WT and *Prph*KO mice by ABR (Figure 9). WT and *Prph*KO mice had equivalent pre-noise ABR thresholds for click and tone-pip stimuli (4–32 kHz)

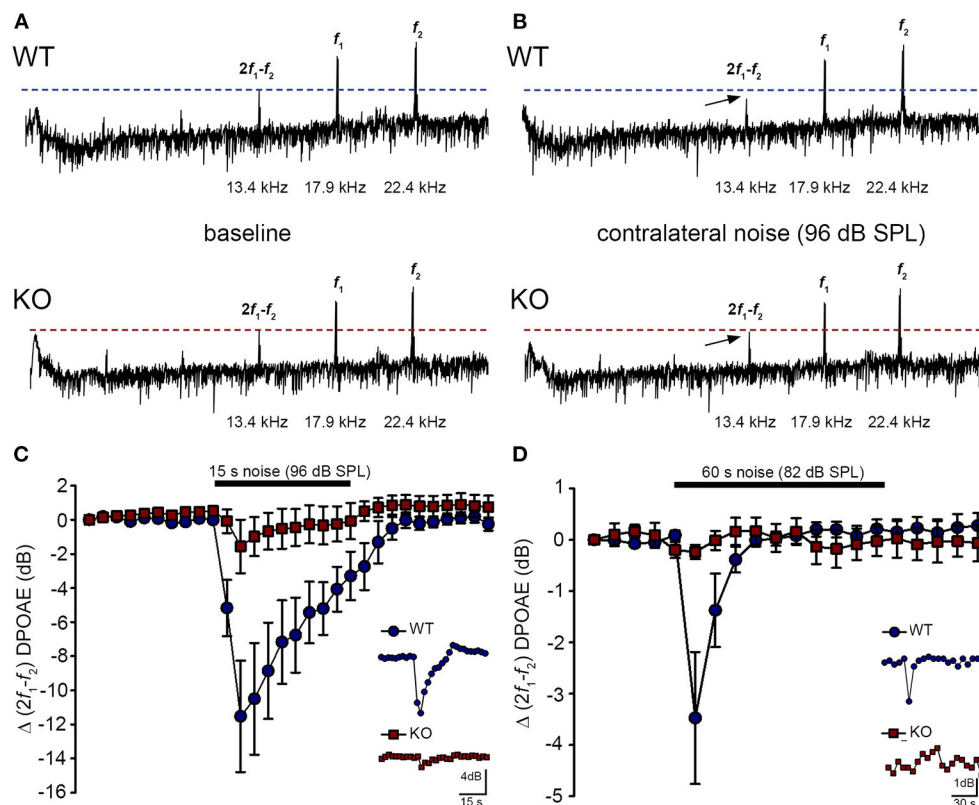


FIGURE 7

Contralateral suppression (CS) of the cubic ($2f_1 - f_2$) DPOAE in wildtype (WT) and *Prph*KO mice under ketamine/xylazine/acepromazine anesthesia. (A,B), Examples of fast Fourier transforms of the DPOAE in the frequency domain with WT and KO at baseline (A,B) with the presentation of contralateral noise (96 dB SPL, 15–25 kHz, 15 s duration, with f_1 and f_2 about 20 kHz using 60 dB SPL drivers). The cubic DPOAE (arrows) is diminished in the WT mouse (contralateral suppression) but is not affected in the KO mouse. (C) Data showing the difference in contralateral suppression with presentation of 96 dB SPL white noise in the WT mice and KO mice. Note the rapid onset to peak contralateral suppression at ~ 3 s, followed by almost complete adaptation by 15 s (unpaired *t*-test; $n = 7$ per group). (D) Difference in contralateral suppression between WT and KO mice during 82 dB SPL noise (60 s, about 10–17 kHz, with f_1 and f_2 about 28 kHz using 65 dB SPL drivers). Note the complete adaptation by ~ 30 s in the WT mice, whereas the DPOAE is unchanged in the KO mice (unpaired *t*-test; $n = 8$ per group).

(Figure 9A), which indicates that disruption of the type II SGN sensory drive does not affect hearing sensitivity in a nominally quiet environment. Pre-noise click input-output functions were also equivalent (click ABR: 0.062 ± 0.009 $\mu\text{V}/\text{dB}$ WT; 0.078 ± 0.011 $\mu\text{V}/\text{dB}$ *Prph*KO; $p = 0.277$, *t*-test; $n = 9$ per group). ABR threshold shifts immediately after noise exposure were comparable between the WT and *Prph*KO mice, with the greatest changes (~ 60 – 70 dB) observed from 16–32 kHz (Figure 9B). Permanent hearing loss (permanent threshold shift–PTS), was determined by re-measurement of ABR thresholds 2 weeks after noise exposure. While the WT mice did not exhibit any significant PTS, with thresholds returning to pre-noise baseline, the *Prph*KO mice exhibited high frequency hearing loss, with PTS of 10.9 ± 2.0 dB at 24 kHz and 19.4 ± 5.1 dB at 32 kHz [$p < 0.016$; Two-way RM ANOVA; $n = 9$ per genotype (Figure 9C)]. Data distribution from individual animals at 24 kHz and 32 kHz

shown in boxplots (Supplementary material 10). The Power of the two-way ANOVA analysis of genotype effect on noise-induced hearing loss was 0.655 with $\alpha = 0.05$. The ABR input/output functions for neural recruitment of the WT mice, and *Prph*KO mice 2 weeks post-noise, demonstrated equivalency at frequencies where the *Prph*KO mice exhibited significant threshold shifts (Supplementary material 11). The average slopes for 24 kHz were: WT = 0.032 ± 0.002 $\mu\text{V}/\text{dB}$; *Prph*KO = 0.038 ± 0.005 $\mu\text{V}/\text{dB}$. 32 kHz slopes were: WT = 0.032 ± 0.003 $\mu\text{V}/\text{dB}$; *Prph*KO = 0.038 ± 0.005 $\mu\text{V}/\text{dB}$ (two-way RM ANOVA for genotype comparison, $p > 0.05$). Supporting comparable ABR input/output functions; cubic DPOAE (8 kHz, 12 kHz, 16 kHz, 24 kHz, and 32 kHz) at 2 weeks post-noise showed no significant differences in thresholds (respective difference of means: 2.22 dB, 1.11 dB, 4.44 dB, 5.00 dB, 8.33 dB); $p > 0.05$ two-way RM ANOVA; input/output functions ($p > 0.05$ two-way RM ANOVA); consistent with

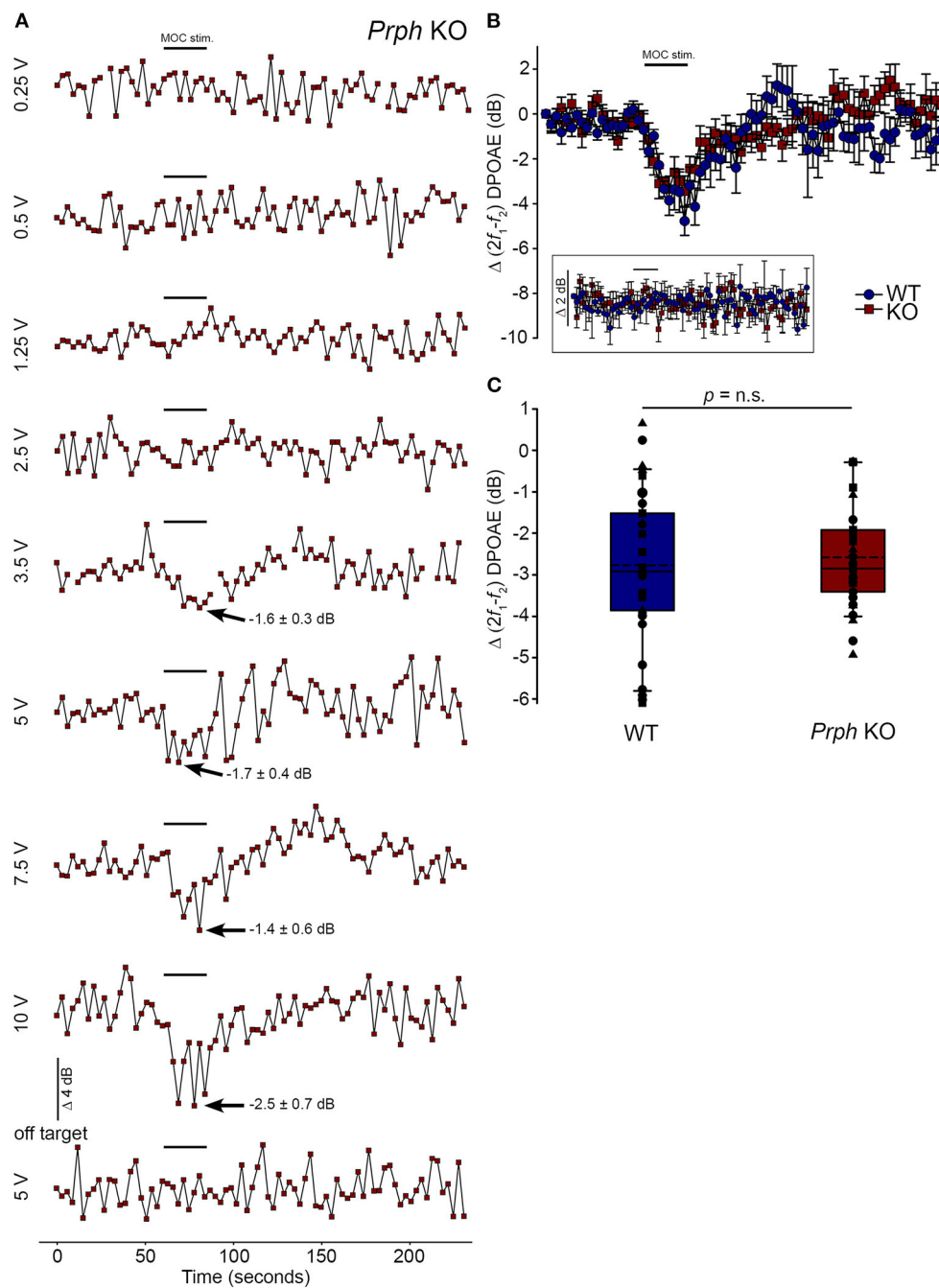
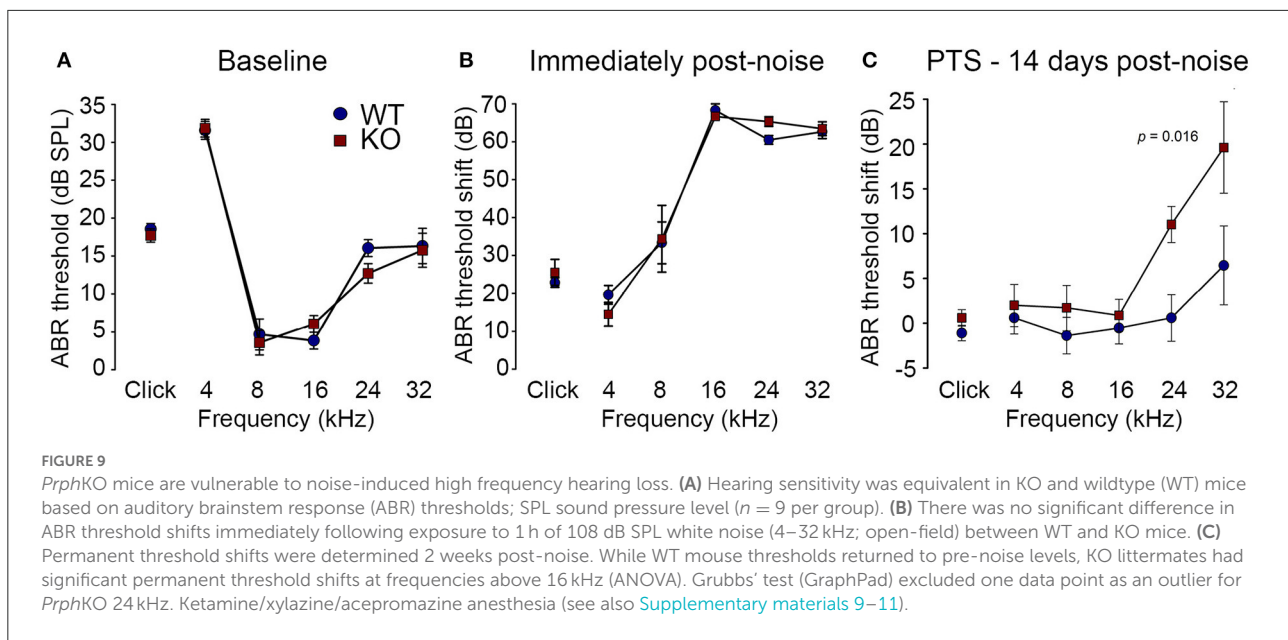


FIGURE 8

Equivalency of electrically-evoked DPOAE suppression in *Prph*KO and wildtype (WT) mice under isoflurane anesthesia. **(A)** Baseline cubic DPOAE ($2f_1-f_2$) with f_1 and f_2 primaries around 16 kHz at 50–55 dB SPL was established using 3 s repeated sampling for 60 s, followed by 25 s of direct electrical stimulation of the crossed olivocochlear bundle fibers on the floor of the brainstem fourth ventricle (medial olivocochlear efferent stimulation (MOC stim.), black bar; monophasic pulses, 150 μ s duration, 200 Hz), and then 150 s of recovery (*Prph*KO mouse). The bottom trace (“off-target”) illustrates a “false-negative” outcome (a 2 mm rostral repositioning of the probe eliminated the suppression of DPOAE elicited with an equivalent 5 V stimulus level). Arrows indicate average contralateral suppression over the stimulus period relative to the preceding baseline average. **(B)** Overlay of the averaged electrically-evoked DPOAE suppression responses for WT and KO mice. The data show the mean and S.E.M. based on 3–5 repeated MOC stimuli for each mouse, with 25 s electrical stimulation at suprathreshold stimulus voltages (WT 5 V, $n = 3$; KO 2–8 V, $n = 3$). The inset shows stability of the recordings with subthreshold stimulation (0.25–1 V). **(C)** Boxplots show the equivalency of the average electrically-evoked DPOAE suppressions, with 25 and 75% boundaries and bars to 95% confidence limits. Individual data overlaid (symbols show repeats for individual mice); dashed lines show the mean; solid lines show the median. $p = n.s.$ indicates $p > 0.05$, by repeated measure two-way ANOVA.



preservation of OHCs and potential type I afferent synaptopathy underlying the ABR PTS.

The potential for noise-induced hair cell loss and synaptopathy in the basal cochlea region, anatomically mapped to the observed high frequency PTS (38), was examined in cryosections from 3 WT and 2 *Prph*KO mice following the 2 week post-noise PTS assessment. Myosin 7A immunolabelling confirmed OHC and IHC preservation ([Supplementary material 12](#)). Similarly nominal pre-synaptic ribbon presentation at the base of the IHCs in WT and *Prph*KO noise-exposed tissue was maintained based on CtBP2 immunofluorescence ([Supplementary material 12](#)). The pre-synaptic ribbons maintained close juxtaposition to post-synaptic GluA2 type I afferent terminals at the IHC, consistent with preserved function ([Supplementary material 12](#)). Irregular localization of *Prph*KO OHC CtBP2 immunopositive ribbons was anticipated by the phenotype [compare ([Supplementary material 12](#))]. The lack sensitivity in identifying putative hair cell cytopathology is consistent with the modest discrete PTS generated by the noise challenge (39, 40).

Discussion

These studies provide strong evidence that at loud sound levels, the OHC–type II SGN afferent input to the cochlear nucleus contributes to the activation of the MOC efferent feedback control of the cochlear amplifier to confer protection from noise-induced hearing loss. Hearing sensitivity (threshold ABR and DPOAE amplitude) is equivalent for WT and

Prph deficient mice. However, in the *Prph*KO, acoustically-evoked contralateral suppression was absent at 82 dB SPL noise (just above the threshold for detectable WT contralateral suppression), and was ~ 10 dB less than WT using high level (96 dB SPL) noise (where 3 dB represents a halving of intensity). These measurements were undertaken at 20–28 kHz, probing the middle region of the mouse cochlea (41). The region exhibits profound type II SGN dendrite dysmorphology in the *Prph*KO cochlea ([Figure 3B](#)), with only residual outer spiral fibers in evidence, and OHC synaptic ribbons significantly displaced.

Our initial NF200 immunolabelling in adult *Prph*KO cochlea identified the significant reduction in the number of outer spiral fibers (23). This phenotypic characteristic was subsequently disputed by Maison et al. (11), who reported a normal OSB structure, and the stereotypical localization of the OHC CtBP2-immunopositive pre-synaptic ribbons, in their *Prph*KO mice. In the present study, we validated the characterization of the abnormal OSB fiber phenotype in our *Prph*KO mouse model using NF200, β -III tubulin, and parvalbumin immunofluorescence modalities. CtBP2 immunolabelling of the OHC pre-synaptic ribbons showed evident disruption (apical drift) from the ordered basal localization in the WT, consistent with deafferentation (32). This observation was statistically validated by the blinded study that measured the position of several hundred WT and *Prph*KO CtBP2 positive pre-synaptic ribbons with respect to OHC nucleus equator, across 5 WT and 6 *Prph*KO mice ([Supplementary material 8](#)). The finding of loss of tethering of the pre-synaptic ribbons in the *Prph*KO OHC supports our previous characterization of the (post-synaptic) afferent bouton structure using serial blockface scanning electron microscopy

(23), (Supplementary Figure 2 and Supplementary Table 1). In that study no type II SGN afferent boutons could be identified in synaptic contact with *Prph*KO OHCs, compared to 1–2 reconstructed afferent terminals per WT OHC; consistent with other mouse data (19, 42). In the same WT and *Prph*KO samples, ~ 2.3 MOC efferent boutons were rendered per OHC for both genotypes (23). Outside of a potential tissue genotyping mismatch, it does not seem possible to reconcile the structural anomaly in the type II afferent innervation of the OHCs which we have detailed across our studies, with the Maison et al. (11) report. In addition to Froud et al. (23), we have also previously demonstrated that the knockout of peripherin expression altered regulation of type II afferent neurite growth in an *in vitro* neonatal cochlear spiral ganglion explant model (43); a finding congruent with the anomalous outer spiral bundle structure in the adult *Prph*KO mice.

Disruption of type II SGN afferent neurites in the *Prph*KO cochlea is consistent with evidence that the type III intermediate filament protein peripherin supports axon growth and synaptic consolidation, particularly in sensory fibers of the peripheral nervous system (44–46). *Prph* knockout was originally reported to cause selective loss of small diameter unmyelinated nociceptor dorsal root ganglion (DRG) fibers, while sparing the majority of peripherin-positive DRG neurons (28). This variation in impact of *Prph* gene deletion has been linked to co-regulation of complementary type IV intermediate filaments, α -internexin and neurofilament proteins (particularly NF-L) which jointly contribute to nerve fiber outgrowth, branching and synapse formation (28, 47, 48). On this basis, the selective impact of *Prph*KO on the mouse cochlear type II SGN innervation of the OHCs may reflect insufficiency of compensation from co-expressed neurofilaments. In the brain, *Prph* expression is largely constrained to cranial nerve sensori-motor pathways, such as the mesencephalic trigeminal nucleus (49). Injury stimulates *de novo* expression of peripherin in the brain, leading to aggregation of the protein and neurodegeneration (50). Upregulation of *Prph* expression contributes to injury repair responses in the peripheral nervous system, for example, being linked to axon regrowth and sprouting following sciatic nerve crush (51). While largely conserved across species, peripherin expression does exhibit spatiotemporal variations across tissues likely associated with variations in promoter and regulatory domains (46). In the rat cochlea, peripherin expression overlaps with type I SGN for several days beyond birth (52), while in the mouse, peripherin is strongly biased to the unmyelinated type II SGN, over type I SGN from \sim E18 onwards, and is most strongly represented in those OSB fibers during early post-natal neurite extension and synaptic consolidation across the first post-natal week (24, 25, 53).

In vivo electrophysiological studies of type II SGN are limited, but suggest that these small, unmyelinated neurons have slow conduction velocities, high thresholds and relative

insensitivity to sound stimulation. Robertson (54) delivered horseradish peroxidase during intracellular high-impedance microelectrode recordings of SGN somata in the guinea pig Rosenthal's canal to definitively label an outer spiral fiber projecting to basal OHCs. Unlike type I SGN, which project as radial fibers to IHCs and respond to sound stimulation, this single labelled type II SGN was "silent" (54). The more definitive data of Brown (21) is from 19 putative guinea pig type II units recorded with high impedance glass microelectrodes. These unlabelled, but presumed type II SGN, were characterized by longer antidromic response latencies than type I SGN units. Some responded to acoustic stimulation, with the most sensitive threshold at 80 dB SPL, matching the current contralateral suppression paradigm. Units with the longest antidromic latencies were generally unresponsive to sound. In a subsequent guinea pig study (55), additional SGN recordings from "silent" units with long antidromic stimulus latencies were evaluated, but the identity and integrity of these cells was questioned.

Additional studies of type II SGN physiology have been performed *in vitro*. *In situ* whole-cell patch-clamp analysis in a rat neonatal cochlear slice preparation showed comparable recruitment of action potentials in type I and type II SGN, with an A-type inactivating K^+ channel conductance prominent in the type II SGN, with reduced AMPA-type glutamate receptor conductance, but comparable ATP-activated inward currents (20). Type II SGN had significantly depolarized resting potentials compared with type I SGN, which may explain the limited ability to record action potentials from these neurons *in vivo* with microelectrodes. Under current-clamp, isolated mouse type II SGN exhibited region-dependent variation in firing properties similar to those of type I SGN (56). Patch-clamp recordings of neonatal rat type II SGN terminal processes provided definitive evidence of OHC glutamatergic neurotransmission and purinergic neuromodulation, including spontaneous excitatory post-synaptic potentials/currents (EPSP/EPSC) (57). Glutamatergic transmission appeared weaker than that of IHC-type I SGN synapses, based on the limited number of spontaneous EPSC events. These studies were extended and showed synaptic transmission *via* GluA2-containing AMPA receptors evoked by local application of K^+ . The data are consistent with a requirement for integrated summation of synaptic transmission from ~ 6 OHCs to reach action potential threshold, sustained by an outer spiral fiber length constant beyond 1 mm, and supported by $Na_v1.6$ voltage-gated Na^+ channels (5, 58, 59).

There is overlapping distribution of type I and type II spiral ganglion afferent input to the cochlear nucleus. Both type I and type II SGN have branching termination in the dorsal and ventral cochlear nuclei, with type II SGN having considerable additional input to the cochlear nucleus granule cell region, a feature lacking in type I SGN (17). In the

small cell region in the posteroventral cochlear nucleus region (PVCN) immediately adjacent to the granule cell domain (60), electron microscopy localized type II synapses on stellate cells (61). This region also receives high-threshold type I auditory nerve fibers (62), has high-threshold auditory neurons (63), and projects to the olivocochlear neurons (64, 65). Darrow et al. (66) used dye injections into the mouse cochlea for retrograde labeling of contralateral MOC efferent neurons in the ventral nucleus of the trapezoid body, alongside anterograde labeling from the PVCN that resolved planar stellate cells synapsing onto those MOC somata and dendrites; local PVCN ablation reduces MOC reflex suppression (10). Alongside this, studies across species have identified reciprocal connectivity between the MOC neurons and the cochlear nuclei, reflecting complexity of afferent and efferent circuitry regulating the MOC reflex (65, 67, 68). A notable finding in the gerbil (69) and mouse (70) is that MOC efferent collaterals project to the cochlear nucleus granule cell region, a selective convergence with type II SGN afferent input. In support of the *in vivo* electrophysiological findings for type II SGN functionality, using noxious noise levels Flores et al. (71) reported increase in *cFos* signal in the cochlear nucleus granule cell region in *VGlut3* KO mice, which lack IHC–type I SGN transmission. This finding has been advanced by a more definitive study which selectively modulated OHC glutamatergic neurotransmission to demonstrate functional sensory drive by type II SGN afferents to the granule cell region of the cochlear nucleus spanning moderate (80 dB SPL) to damaging (115 dB SPL) sound levels (16).

It is clear from the present study that the loss of acoustically-evoked contralateral suppression in the *Prph*KO mice occurs upstream of the superior olivary complex, in the afferent supply to the reflex, since the COCB remains functional. This is counter to the Maison et al. (11) *Prph*KO study, which did not observe the type II SGN morphological disruption, and where a negative result for electrically-evoked COCB suppression of the DPOAE in two *Prph*KO mice led to an inference that loss of contralateral suppression likely arose from failure of the efferent arm of the circuit. The present study verifies type II SGN synapse disruption and dendrite loss in the *Prph*KO mouse line. With the strong evidence (16) that type II SGN are acoustically active at moderate and high sound levels, the loss of contralateral suppression in the *Prph*KO mice seems likely due to the type II SGN synapse disruption. A radical change in drive from the IHC–type I afferent sensory input in the *Prph*KO mouse appears less likely, since hearing sensitivity is maintained. The possibility of selective loss of a subset of high threshold afferent input to the MOC region such as the the PVCN small cells which connect reciprocally is also a possibility, but there is no evidence for peripherin expression in the cochlear nucleus (49). Other alternatives are possible. A small number of the MOC tunnel crossing fibers were reported as

peripherin immunopositive in wildtype mice (11), although we show here that the electrically-evoked MOC drive for DPOAE suppression was equivalent in the *Prph*KO. In the cochlea, type II SGN fibers make terminal arborizations with Deiters' and Hensen's cells, particularly in the apical region, although it is uncertain whether these reflect synaptic couplings (72). Reciprocal transmission between type II SGN afferents and the OHCs, evident from electron microscopy studies in cat and primates, could also contribute to local integration of OHC sensory transduction (73). There are also synaptic varicosities between type II SGN afferents and the MOC efferent terminals (74) which may support GABAergic transmission as part of a reciprocal microcircuit in the early post-natal period in rats (75). Changes in these cochlear connections could potentially be a factor.

Any of these potential mechanisms demonstrate a critical role for peripherin in afferent feed to contralateral suppression. However, in the absence of evidence supporting alternatives, we feel that parsimony favors loss of OHC–type II SGN input as the root cause of loss of contralateral suppression with 82–96 dB SPL broadband noise range tested here. This postulate is arguably most strongly supported by a complementary mouse study that selectively reduced IHC–type I afferent input to the cochlear nucleus by treating the cochlear round window membrane with ouabain, causing ~ 90% reduction in the ABR wave I amplitude, but preserved contralateral suppression using 76 dB SPL broadband noise (15).

Given the long-standing evidence that type I SGN afferent input drives the MOC efferents, based on near-equivalency of single fiber thresholds and tuning characteristics (12, 13), the association here of disruption of type II SGN input and loss of contralateral suppression suggests that the broad reduction of the cochlear amplifier by the COCB at higher noise levels, captured by DPOAE, may require the combined drive of both type I SGN and type II SGN input, with the unexpected finding that type I SGN drive alone may fall short with regard to the role of the MOC feedback circuit for protection of the hair cells and their synapses from acoustic overstimulation. It is well established that MOC efferent feedback is critical to the long-term protection of the cochlear hair cells and their afferent innervation (4). For example, chronic moderate (84 dB SPL) noise exposure caused increased type I SGN synaptopathy in mice when the COCB was sectioned at the floor of the fourth ventricle (76). MOC efferent-mediated protection from NIHL has been confirmed in mice using selective genetic manipulation of the OHC nicotinic cholinergic receptor (nAChR). As noted above, a gain of function mutation of the $\alpha 9$ nAChR subunit confers heightened resistance to NIHL (77, 78), as does $\alpha 9$ nAChR subunit overexpression (37). Knockout of the $\alpha 9$ nAChR subunit enhances NIHL (78). That study in the $\alpha 9$ nAChR KO utilized a lower frequency noise band (1–16 kHz, 100 dB SPL, 1 h, open field,

with ketamine/xylazine anesthesia) than the present study and achieved higher broad sustained threshold shifts (averaging up to 35 dB compared with no PTS in WT mice). While no hair cell loss was detectable, a quantitative analysis of CtBP2 and GluA2 IHC synapse immunofluorescence across hundreds of IHCs in whole-mount preparations resolved significant synaptopathy. Given that our ABR PTS shifts were smaller and our study was not powered to quantitatively assess synaptic integrity, the NIHL associated with the *Prph*KO-mediated disruption of the MOC reflex most likely stems from similar synaptopathy.

These findings provide a clear imperative for development of more sophisticated models for selective manipulation of the two cochlear afferent populations to probe the sensory drive of the MOC efferent control of the cochlear amplifier. This challenge may be met in part by leveraging the use of *Prph* gene targeting by integrating Bacterial Artificial Chromosomes (BAC) in transgenic mice. For example, a mouse line integrating a 150 kb BAC containing the human *PRPH* gene and associated promoter and regulatory non-coding regions engineered to generate a (functional) peripherin fusion protein with enhanced green fluorescent protein (*PRPH-eGFP*) (46) has proved to be an effective type II SGN afferent biomarker, with strong correlation to native mouse cochlear peripherin immunolabelling (53). While crossing of this mouse model to the current *Prph*KO mouse line would retain peripherin protein translation (from the BAC *PRPH* expression); modification of this BAC, or a similar mouse *Prph* BAC as developed by the Gene Expression Nervous System Atlas (GENSAT) program (79), to integrate a conditional human diphtheria toxin receptor (hDTR) transgene element into the *Prph* reading frame, may allow selective ablation of the adult cochlea type II SGN, extending functional insight into the role(s) of the OHC-type II SGN afferent pathway in hearing.

In summary, in the *Prph*KO mouse model, we demonstrate clear association between the disruption of OHC-type II SGN sensory input, near-elimination of MOC efferent-mediated contralateral suppression at moderate to high sound levels, and reduction in otoprotection against NIHL. The findings support the contribution of cochlear OHC-type II SGN afferents to the sensory drive of the MOC efferent suppression of the cochlear amplifier that confers noise-induced hearing loss protection.

Data availability statement

The original contributions presented in the study are included in the article/Supplementary material, further inquiries can be directed to the corresponding author/s.

Ethics statement

The animal study was reviewed and approved by UNSW Sydney Animal Care and Ethics Committee.

Author contributions

JC, KP, GH, AR, and J-PJ contributed to the conception and design of the study. JC, KP, JP, and GH undertook the physiological studies. JC, KP, CP, GJ, DR, AR, and GH performed the histological and imaging studies and structural analysis. GH, AR, and DR contributed to the funding. All authors contributed to the data validation and presentation, production of the manuscript, and approved the submitted version.

Funding

This work was supported by Australia grants from the National Health & Medical Research Council (NHMRC) APP1052463, APP1189113, and APP1188643 & U.S. Department of Veterans Affairs grants BX001205 and RX002704. The authors declare that this study also received funding from Alan and Lynne Rydge to the Hearing Research Lab at the Garvan Institute. They were not involved in the study design, collection, analysis, interpretation of data, the writing of this article or the decision to submit it for publication.

Acknowledgments

Edward Crawford is thanked for his contributions to development of the instrumentation and software for the study.

Conflict of interest

Author AR is a co-founder of Otonomy Inc., serves as a member of the Scientific Advisory Board, and holds an equity position in the company. The UCSD Committee on Conflict of Interest has approved this relationship. Otonomy, Inc. played no part in the research reported here.

The remaining authors declare that the research was conducted in the absence of any commercial or financial relationships that could be construed as a potential conflict of interest.

Publisher's note

All claims expressed in this article are solely those of the authors and do not necessarily represent those

of their affiliated organizations, or those of the publisher, the editors and the reviewers. Any product that may be evaluated in this article, or claim that may be made by its manufacturer, is not guaranteed or endorsed by the publisher.

References

- Ryan A, Dallos P. Effect of absence of cochlear outer hair cells on behavioural auditory threshold. *Nature*. (1975) 253:44–6. doi: 10.1038/253044a0
- Ashmore J. Outer hair cells and electromotility. *Cold Spring Harb Perspect Med*. (2019) 9:a033522. doi: 10.1101/cshperspect.a033522
- Lopez-Poveda EA. Olivocochlear efferents in animals and humans: From anatomy to clinical relevance. *Front Neurol*. (2018) 9:197. doi: 10.3389/fneur.2018.00197
- Fuchs PA, Lauer AM. Efferent inhibition of the cochlea. *Cold Spring Harb Perspect Med*. (2019) 9:a033530. doi: 10.1101/cshperspect.a033530
- Weisz CJ, Lehar M, Hiel H, Glowatzki E, Fuchs PA. Synaptic transfer from outer hair cells to type II afferent fibers in the rat cochlea. *J Neurosci*. (2012) 32:9528–36. doi: 10.1523/JNEUROSCI.6194-11.2012
- Brown MC. Single-unit labeling of medial olivocochlear neurons: the cochlear frequency map for efferent axons. *J Neurophysiol*. (2014) 111:2177–86. doi: 10.1152/jn.00045.2014
- Althen H, Wittekindt A, Gaese B, Kossel M, Abel C. Effect of contralateral pure tone stimulation on distortion emissions suggests a frequency-specific functioning of the efferent cochlear control. *J Neurophysiol*. (2012) 107:1962–9. doi: 10.1152/jn.00418.2011
- Maison SF, Usubuchi H, Vetter DE, Elgoyhen AB, Thomas SA, Liberman MC. Contralateral-noise effects on cochlear responses in anesthetized mice are dominated by feedback from an unknown pathway. *J Neurophysiol*. (2012) 108:491–500. doi: 10.1152/jn.01050.2011
- Brown MC, Mukerji S, Drottar M, Windsor AM, Lee DJ. Identification of inputs to olivocochlear neurons using transneuronal labeling with pseudorabies virus (PRV). *J Assoc Res Otolaryngol*. (2013) 14:703–17. doi: 10.1007/s10162-013-0400-5
- Brown MC, De Venecia RK, Guinan JJJr. Responses of medial olivocochlear neurons. Specifying the central pathways of the medial olivocochlear reflex. *Exp Brain Res*. (2003) 153:491–8. doi: 10.1007/s00221-003-1679-y
- Maison S, Liberman LD, Liberman MC. Type II cochlear ganglion neurons do not drive the olivocochlear reflex: Re-examination of the cochlear phenotype in peripherin knock-out mice. *eNeuro*. (2016) 3:ENEURO.0207-16.2016. doi: 10.1523/ENEURO.0207-16.2016
- Robertson D, Gummer M. Physiological and morphological characterization of efferent neurones in the guinea pig cochlea. *Hear Res*. (1985) 20:63–77. doi: 10.1016/0378-5955(85)90059-0
- Liberman MC, Brown MC. Physiology and anatomy of single olivocochlear neurons in the cat. *Hear Res*. (1986) 24:17–36. doi: 10.1016/0378-5955(86)90003-1
- Park SY, Park JM, Back SA, Yeo SW, Park SN. Functional significance of medial olivocochlear system morphology in the mouse cochlea. *Clin Exp Otorhinolaryngol*. (2017) 10:137–42. doi: 10.21053/ceo.2016.00444
- Li J, Chen Y, Zeng S, Lai C, Zhang Y, Zhang L, et al. Contralateral suppression of DPOAEs in mice after ouabain treatment. *Neural Plast*. (2018) 2018:6890613. doi: 10.1155/2018/6890613
- Weisz CJC, Williams SG, Eckard CS, Divito CB, Ferreira DW, Fantetti KN, et al. Outer hair cell glutamate signaling through type II spiral ganglion afferents activates neurons in the cochlear nucleus in response to nondamaging sounds. *J Neurosci*. (2021) 41:2930–43. doi: 10.1523/JNEUROSCI.0619-20.2021
- Brown MC, Berglund AM, Kiang NY, Ryugo DK. Central trajectories of type II spiral ganglion neurons. *J Comp Neurol*. (1988) 278:581–90. doi: 10.1002/cne.902780409
- Barclay M, Ryan AF, Housley GD. Type I vs type II spiral ganglion neurons exhibit differential survival and neurogenesis during cochlear development. *Neural Dev*. (2011) 6:33. doi: 10.1186/1749-8104-6-33
- Berglund AM, Ryugo DK. Hair cell innervation by spiral ganglion neurons in the mouse. *J Comp Neurol*. (1987) 255:560–70. doi: 10.1002/cne.902550408
- Jagger DJ, Housley GD. Membrane properties of type II spiral ganglion neurones identified in a neonatal rat cochlear slice. *J Physiol*. (2003) 552:525–33. doi: 10.1111/j.1469-7793.2003.00525.x
- Brown MC. Antidromic responses of single units from the spiral ganglion. *J Neurophysiol*. (1994) 71:1835–47. doi: 10.1152/jn.1994.71.5.1835
- Kim DO. Active and nonlinear cochlear biomechanics and the role of outer-hair-cell subsystem in the mammalian auditory system. *Hear Res*. (1986) 22:105–14. doi: 10.1016/0378-5955(86)90088-2
- Froud KE, Wong AC, Cederholm JM, Klugmann M, Sandow SL, Julien JP, et al. Type II spiral ganglion afferent neurons drive medial olivocochlear reflex suppression of the cochlear amplifier. *Nat Commun*. (2015) 6:7115. doi: 10.1038/ncomms8115
- Huang LC, Thorne PR, Housley GD, Montgomery JM. Spatiotemporal definition of neurite outgrowth, refinement and retraction in the developing mouse cochlea. *Development*. (2007) 134:2925–33. doi: 10.1242/dev.001925
- Huang LC, Barclay M, Lee K, Peter S, Housley GD, Thorne PR, et al. Synaptic profiles during neurite extension, refinement and retraction in the developing cochlea. *Neural Dev*. (2012) 7:38. doi: 10.1186/1749-8104-7-38
- Nhmrc (2013). Australian code for the care and use of animals for scientific purposes. In: *Australian Federal Government National Health and Medical Research Council 8th Edition*, ISBN 1864965975.
- Kilkenny C, Browne WJ, Cuthill IC, Emerson M, Altman DG. Improving bioscience research reporting: the ARRIVE guidelines for reporting animal research. *PLoS Biol*. (2010) 8:e1000412. doi: 10.1371/journal.pbio.1000412
- Lariviere RC, Nguyen MD, Ribeiro-Da-Silva A, Julien JP. Reduced number of unmyelinated sensory axons in peripherin null mice. *J Neurochem*. (2002) 81:525–32. doi: 10.1046/j.1471-4159.2002.00853.x
- Schmitz F, Königstorfer A, Sudhof TC. RIBEYE, a component of synaptic ribbons: a protein's journey through evolution provides insight into synaptic ribbon function. *Neuron*. (2000) 28:857–72. doi: 10.1016/S0896-6273(00)00159-8
- Cederholm JME, Froud KE, Wong AC, Ko M, Ryan AF, Housley GD. Differential actions of isoflurane and ketamine-based anaesthetics on cochlear function in the mouse. *Hear Res*. (2012) 293:71–79. doi: 10.1016/j.heares.2012.08.010
- Wang Y, Hirose K, Liberman MC. Dynamics of noise-induced cellular injury and repair in the mouse cochlea. *J Assoc Res Otolaryngol*. (2002) 3:248–68. doi: 10.1007/s101620020028
- Singer W, Zuccotti A, Jaumann M, Lee SC, Panford-Walsh R, Xiong H, et al. Noise-induced inner hair cell ribbon loss disturbs central arc mobilization: a novel molecular paradigm for understanding tinnitus. *Mol Neurobiol*. (2013) 47:261–79. doi: 10.1007/s12035-012-8372-8
- Frank G, Kossel M. The acoustic two-tone distortions 2f1-f2 and f2-f1 and their possible relation to changes in the operating point of the cochlear amplifier. *Hear Res*. (1996) 98:104–15. doi: 10.1016/0378-5955(96)00083-4
- Mills DM, Rubel EW. Development of the cochlear amplifier. *J Acoust Soc Am*. (1996) 100:428–41. doi: 10.1121/1.415857
- Housley GD, von Jonquieres G, Pinyon JL, Matheson JA, Pearson LJ, Salthouse TP, et al. Cochlear homeostasis: a molecular physiological perspective on maintenance of sound transduction and auditory neurotransmission with noise and ageing. *Current Opin Physiol*. (2020) 18:106–115. doi: 10.1016/j.cophys.2020.09.012
- Rajan R. Centrifugal pathways protect hearing sensitivity at the cochlea in noisy environments that exacerbate the damage induced by loud sound. *J Neurosci*. (2000) 20:6684–93. doi: 10.1523/JNEUROSCI.20-17-06684.2000
- Maison SF, Luebke AE, Liberman MC, Zuo J. Efferent protection from acoustic injury is mediated via alpha9 nicotinic

Supplementary material

The Supplementary Material for this article can be found online at: <https://www.frontiersin.org/articles/10.3389/fneur.2022.962227/full#supplementary-material>

- acetylcholine receptors on outer hair cells. *J Neurosci.* (2002) 22:10838–46. doi: 10.1523/JNEUROSCI.22-24-10838.2002
38. Ou HC, Harding GW, Bohne BA. An anatomically based frequency-place map for the mouse cochlea. *Hear Res.* (2000) 145:123–9. doi: 10.1016/S0378-5955(00)00082-4
 39. Ou HC, Bohne BA, Harding GW. Noise damage in the C57BL/CBA mouse cochlea. *Hear Res.* (2000) 145:111–22. doi: 10.1016/S0378-5955(00)00081-2
 40. Wang Y, Liberman MC. Restraint stress and protection from acoustic injury in mice. *Hear Res.* (2002) 165:96–102. doi: 10.1016/S0378-5955(02)00289-7
 41. Muller M, Von Hunerbein K, Hoidis S, Smolders JW. A physiological place-frequency map of the cochlea in the CBA/J mouse. *Hear Res.* (2005) 202:63–73. doi: 10.1016/j.heares.2004.08.011
 42. Wood MB, Nowak N, Mull K, Goldring A, Lehar M, Fuchs PA. Acoustic trauma increases ribbon number and size in outer hair cells of the mouse cochlea. *J Assoc Res Otolaryngol.* (2021) 22:19–31. doi: 10.1007/s10162-020-00777-w
 43. Barclay M, Julien JP, Ryan AF, Housley GD. Type III intermediate filament peripherin inhibits neurogenesis in type II spiral ganglion neurons in vitro. *Neurosci Lett.* (2010) 478:51–5. doi: 10.1016/j.neulet.2010.01.063
 44. Helfand BT, Mendez MG, Pugh J, Delsert C, Goldman RD. A role for intermediate filaments in determining and maintaining the shape of nerve cells. *Mol Biol Cell.* (2003) 14:5069–81. doi: 10.1091/mbc.e03-06-0376
 45. Lariviere RC, Julien JP. Functions of intermediate filaments in neuronal development and disease. *J Neurobiol.* (2004) 58:131–48. doi: 10.1002/neu.10270
 46. Mclenachan S, Goldshmit Y, Fowler KJ, Voullaire L, Holloway TP, Turnley AM, et al. Transgenic mice expressing the Peripherin-EGFP genomic reporter display intrinsic peripheral nervous system fluorescence. *Transgenic Res.* (2008) 17:1103–16. doi: 10.1007/s11248-008-9210-7
 47. Beaulieu JM, Robertson J, Julien JP. Interactions between peripherin and neurofilaments in cultured cells: disruption of peripherin assembly by the NF-M and NF-H subunits. *Biochem Cell Biol.* (1999) 77:41–5. doi: 10.1139/o99-003
 48. Yuan A, Sasaki T, Kumar A, Peterhoff CM, Rao MV, Liem RK, et al. Peripherin is a subunit of peripheral nerve neurofilaments: implications for differential vulnerability of CNS and peripheral nervous system axons. *J Neurosci.* (2012) 32:8501–8. doi: 10.1523/JNEUROSCI.1081-12.2012
 49. Barclay M, Noakes PG, Ryan AF, Julien JP, Housley GD. Neuronal expression of peripherin, a type III intermediate filament protein, in the mouse hindbrain. *Histochem Cell Biol.* (2007) 128:541–50. doi: 10.1007/s00418-007-0340-4
 50. Beaulieu JM, Kriz J, Julien JP. Induction of peripherin expression in subsets of brain neurons after lesion injury or cerebral ischemia. *Brain Res.* (2002) 946:153–61. doi: 10.1016/S0006-8993(02)02830-5
 51. Chadan S, Le Gall JY, Di Giamberardino L, Filliatre G. Axonal transport of type III intermediate filament protein peripherin in intact and regenerating motor axons of the rat sciatic nerve. *J Neurosci Res.* (1994) 39:127–39. doi: 10.1002/jnr.490390203
 52. Hafidi A, Despres G, Romand R. Ontogenesis of type II spiral ganglion neurons during development: peripherin immunohistochemistry. *Int J Dev Neurosci.* (1993) 11:507–12. doi: 10.1016/0736-5748(93)90024-8
 53. Elliott KL, Kersigo J, Lee JH, Jahan I, Pavlinkova G, Fritzsche B, et al. Developmental Changes in Peripherin-eGFP Expression in Spiral Ganglion Neurons. *Front Cell Neurosci.* (2021) 15:678113. doi: 10.3389/fncel.2021.678113
 54. Robertson D. Horseradish peroxidase injection of physiologically characterized afferent and efferent neurones in the guinea pig spiral ganglion. *Hear Res.* (1984) 15:113–21. doi: 10.1016/0378-5955(84)90042-X
 55. Robertson D, Sellick PM, Patuzzi R. The continuing search for outer hair cell afferents in the guinea pig spiral ganglion. *Hear Res.* (1999) 136:151–8. doi: 10.1016/S0378-5955(99)00120-3
 56. Reid MA, Flores-Otero J, Davis RL. Firing patterns of type II spiral ganglion neurons in vitro. *J Neurosci.* (2004) 24:733–42. doi: 10.1523/JNEUROSCI.3923-03.2004
 57. Weisz C, Glowatzki E, Fuchs P. The postsynaptic function of type II cochlear afferents. *Nature.* (2009) 461:1126–9. doi: 10.1038/nature08487
 58. Weisz CJ, Glowatzki E, Fuchs PA. Excitability of type II cochlear afferents. *J Neurosci.* (2014) 34:2365–73. doi: 10.1523/JNEUROSCI.3428-13.2014
 59. Martinez-Monedero R, Liu C, Weisz C, Vyas P, Fuchs PA, Glowatzki E. GluA2-containing AMPA receptors distinguish ribbon-associated from ribbonless afferent contacts on rat cochlear hair cells. *eNeuro.* (2016) 3:ENEURO.0078-16.2016. doi: 10.1523/ENEURO.0078-16.2016
 60. Osen KK. Cytoarchitecture of the cochlear nuclei in the cat. *J Comp Neurol.* (1969) 136:453–84. doi: 10.1002/cne.901360407
 61. Benson TE, Brown MC. Postsynaptic targets of type II auditory nerve fibers in the cochlear nucleus. *J Assoc Res Otolaryngol.* (2004) 5:111–25. doi: 10.1007/s10162-003-4012-3
 62. Ryugo DK. Projections of low spontaneous rate, high threshold auditory nerve fibers to the small cell cap of the cochlear nucleus in cats. *Neuroscience.* (2008) 154:114–26. doi: 10.1016/j.neuroscience.2007.10.052
 63. Ghoshal S, Kim DO. Marginal shell of the anteroventral cochlear nucleus: single-unit response properties in the unanesthetized decerebrate cat. *J Neurophysiol.* (1997) 77:2083–97. doi: 10.1152/jn.1997.77.4.2083
 64. Ye Y, Machado DG, Kim DO. Projection of the marginal shell of the anteroventral cochlear nucleus to olivocochlear neurons in the cat. *J Comp Neurol.* (2000) 420:127–38. doi: 10.1002/(SICI)1096-9861(20000424)420:1<127::AID-CNE9>3.0.CO;2-7
 65. Hockley A, Wu C, Shore SE. Olivocochlear projections contribute to superior intensity coding in cochlear nucleus small cells. *J Physiol.* (2022) 600:61–73. doi: 10.1113/JP282262
 66. Darrow KN, Benson TE, Brown MC. Planar multipolar cells in the cochlear nucleus project to medial olivocochlear neurons in mouse. *J Comp Neurol.* (2012) 520:1365–75. doi: 10.1002/cne.22797
 67. Robertson D, Winter IM. Cochlear nucleus inputs to olivocochlear neurones revealed by combined anterograde and retrograde labelling in the guinea pig. *Brain Res.* (1988) 462:47–55. doi: 10.1016/0006-8993(88)90583-5
 68. Thompson AM, Thompson GC. Projections from the posteroventral cochlear nucleus to the superior olivary complex in guinea pig: light and EM observations with the PHA-L method. *J Comp Neurol.* (1991) 311:495–508. doi: 10.1002/cne.903110405
 69. Ryan AF, Keithley EM, Wang ZX, Schwartz IR. Collaterals from lateral and medial olivocochlear efferent neurons innervate different regions of the cochlear nucleus and adjacent brainstem. *J Comp Neurol.* (1990) 300:572–82. doi: 10.1002/cne.903000410
 70. Brown MC, Liberman MC, Benson TE, Ryugo DK. Brainstem branches from olivocochlear axons in cats and rodents. *J Comp Neurol.* (1988) 278:591–603. doi: 10.1002/cne.902780410
 71. Flores EN, Duggan A, Madathany T, Hogan AK, Marquez FG, Kumar G, et al. A non-canonical pathway from cochlea to brain signals tissue-damaging noise. *Curr Biol.* (2015) 25:606–12. doi: 10.1016/j.cub.2015.01.009
 72. Fechner FP, Nadol JJ, Burgess BJ, Brown MC. Innervation of supporting cells in the apical turns of the guinea pig cochlea is from type II afferent fibers. *J Comp Neurol.* (2001) 429:289–98. doi: 10.1002/1096-9861(2000108)429:2<289::AID-CNE98>3.0.CO;2-Z
 73. Thiers FA, Nadol JBJr, Liberman MC. Reciprocal synapses between outer hair cells and their afferent terminals: evidence for a local neural network in the mammalian cochlea. *J Assoc Res Otolaryngol.* (2008) 9:477–89. doi: 10.1007/s10162-008-0135-x
 74. Ginzberg RD, Morest DK. Fine structure of cochlear innervation in the cat. *Hear Res.* (1984) 14:109–27. doi: 10.1016/0378-5955(84)90011-X
 75. Weisz, C. (2020). Efferent inhibition of type II cochlear afferents. In: *43rd Annual Midwinter Meeting* (Jan Jose, CA: Association for Research in Otolaryngology).
 76. Maison SF, Usubuchi H, Liberman MC. Efferent feedback minimizes cochlear neuropathy from moderate noise exposure. *J Neurosci.* (2013) 33:5542–52. doi: 10.1523/JNEUROSCI.5027-12.2013
 77. Taranda J, Maison SF, Ballester JA, Katz E, Savino J, Vetter DE, et al. A point mutation in the hair cell nicotinic cholinergic receptor prolongs cochlear inhibition and enhances noise protection. *PLoS Biol.* (2009) 7:e18. doi: 10.1371/journal.pbio.1000018
 78. Boero LE, Castagna VC, Di Guilmi MN, Goutman JD, Elgoyhen AB, Gomez-Casati ME. Enhancement of the medial olivocochlear system prevents hidden hearing loss. *J Neurosci.* (2018) 38:7440–51. doi: 10.1523/JNEUROSCI.0363-18.2018
 79. Gong S, Zheng C, Doughty ML, Losos K, Didkovsky N, Schambra UB, et al. A gene expression atlas of the central nervous system based on bacterial artificial chromosomes. *Nature.* (2003) 425:917–25. doi: 10.1038/nature02033